Feed-forward stimulation of CAMK2 by the oncogenic pseudokinase PEAK1 generates a therapeutically 'actionable' signalling axis in triple negative breast cancer

Xue Yang[1,2], Xiuquan Ma[1,2], Tianyue Zhao[1,2], David R Croucher[3,4], Elizabeth V. Nguyen[1,2], Kimberley C. Clark[1,2], Changyuan Hu[1,2], Sharissa L Latham[3,4], Charles Bayly-Jones[1,2], Viet Chi Bao Nguyen[5], Srikanth Budnar[1,2], Sung-Young Shin[1,2], Lan K. Nguyen[1,2], Thomas R. Cotton[1,2], Anderly C. Chüeh[1,2], Terry C C Lim Kam Sian[1,2], Margaret M. Stratton[5], Andrew M. Ellisdon[1,2] and Roger J Daly[1,2,#].

[1]Cancer Program, Monash Biomedicine Discovery Institute, Clayton, VIC 3800, Australia.

[2]Department of Biochemistry and Molecular Biology, Monash University, Melbourne, VIC 3800, Australia.

[3]Garvan Institute of Medical Research, Darlinghurst, NSW 2010, Australia.

[4]St Vincent's Clinical School, Faculty of Medicine, UNSW Sydney, Darlinghurst, NSW 2010, Australia.

[5]Department of Biochemistry and Molecular Biology, University of Massachusetts, Amherst, MA 01003, USA

[#]Correspondence: roger.daly@monash.edu

Summary

The PEAK family of pseudokinases, comprising PEAK1-3, are signalling scaffolds that play oncogenic roles in several poor prognosis human cancers, including triple negative breast cancer (TNBC). However, therapeutic targeting of pseudokinases is challenging due to their lack of catalytic activity. To address this, we screened for PEAK1 effectors by affinity purification and mass spectrometry, identifying calcium/calmodulin-dependent protein kinase 2 (CAMK2)D and CAMK2G. PEAK1 promoted CAMK2D/G activation in TNBC cells via a novel feed-forward mechanism involving PEAK1/PLCγ1/Ca^{2+} signalling and direct binding via a consensus CAMK2 interaction motif in the PEAK1 N-terminus. In turn, CAMK2 phosphorylated PEAK1 to enhance association with PEAK2, which is critical for PEAK1 oncogenic signalling. To achieve pharmacologic targeting of PEAK1/CAMK2, we repurposed RA306, a second generation CAMK2 inhibitor under pre-clinical development for treatment of cardiovascular disease. RA306 demonstrated on-target activity against CAMK2 in TNBC cells and inhibited PEAK1-enhanced migration and invasion *in vitro*. Moreover, RA306 significantly attenuated TNBC xenograft growth and blocked metastasis in a manner mirrored by CRISPR-mediated PEAK1 ablation. Overall, these studies establish PEAK1 as a critical cell signalling nexus, identify a novel mechanism for regulation of Ca^{2+} signalling and its integration with tyrosine kinase signals, and identify CAMK2 as a therapeutically 'actionable' target downstream of PEAK1.

40 **Introduction**

41

42 Pseudokinases play critical roles in normal cellular and developmental processes as well as in
43 human diseases such as cancer, despite lacking the kinase activity of their *bona fide* kinase
44 counterparts. This reflects the ability of pseudokinases to function as allosteric regulators
45 and/or scaffolds that assemble protein signalling complexes[1, 2]. Due to their pathological
46 functions, pseudokinases are attracting increasing attention as therapeutic targets[3].

47

48 The PEAK family of pseudokinases, comprising PEAK1 (previously known as SgK269),
49 PEAK2 (Pragmin and SgK223) and PEAK3 (C19orf35) share a conserved molecular
50 architecture and sequence homology, and function as scaffolds to mediate and regulate
51 signalling downstream of particular growth factor receptors and integrins[4, 5]. PEAK1 is a
52 critical regulator of EGFR signalling, mediating a qualitative shift in signal output over time
53 from mitogenic/survival signalling to that promoting cell migration/invasion[16]. In addition,
54 PEAK1 is strongly implicated in progression of a variety of cancers. For example, in breast
55 cancer, PEAK1 promotes cell proliferation, epithelial-mesenchyme transition (EMT), aberrant
56 acinar morphology in 3D culture and xenograft growth and metastasis[6, 7, 8], in non small cell
57 lung cancer it enhances migration, invasion, EMT and experimental metastasis[9], while in
58 pancreatic cancer models it promotes resistance to specific therapies[10]. Of particular interest,
59 high PEAK1 expression occurs in triple negative breast cancer (TNBC) and pancreatic cancer[6,
60 10], two cancers associated with poor prognosis and limited targeted therapeutic options. PEAK2
61 and PEAK3 also enhance cell migration and invasion and are overexpressed in specific
62 malignancies[4, 11, 12, 13, 14, 15].

63

64 All PEAK family members exhibit a C-terminal pseudokinase domain flanked by a split helical

65 dimerization (SHED) domain, and N-terminal extensions of contrasting length that harbour
66 recruitment sites for specific SH2, SH3 and PTB domain-containing effectors. These effectors
67 include Grb2 (bound by PEAK1 and PEAK3), Shc1 (PEAK1), C-terminal Src kinase (Csk)
68 (PEAK2) and ASAP1, Cbl and PYK2 (PEAK3)[4, 5]. An important characteristic of the PEAK
69 family is their ability to form homotypic and heterotypic complexes[4, 16]. Dimerization of the
70 PEAKs is mediated by the α-helical SHED domain that forms a highly conserved dimer
71 interface driven by hydrophobic interactions[17, 18], while higher order oligomers can also form
72 via pseudokinase domain interfaces[18]. Dimerization is critical to the signalling potential of
73 PEAK scaffolds[4, 12, 18]. Furthermore, since the repertoire of known interactors differs across
74 this family of scaffolds, heterotypic versus homotypic association acts to diversify signal
75 output[4, 16]. For example, PEAK1 requires PEAK2 to efficiently activate Stat3 and promote
76 migration in MCF-10A cells[16, 19], while signalling by PEAK3 is modulated both quantitatively
77 and temporally by the presence of PEAK1 and PEAK2[4].
78
79 In this study, we addressed how homo- and heterotypic association of PEAK1 and PEAK2
80 regulates signal output by defining the interactomes of the corresponding dimeric complexes.
81 Amongst the identified binding interactions, the association of PEAK1 with
82 calcium/calmodulin-dependent protein kinase 2 (CAMK2)D and CAMK2G was of particular
83 interest, given the known roles of specific CAMK2 isoforms in many human cancers, including
84 breast cancer, and the therapeutic 'actionability' of these serine/threonine kinases[20, 21].
85 Importantly, we demonstrate potent, feed-forward activation of CAMK2 by PEAK1,
86 highlighting PEAK1 as a critical regulator and integrator of tyrosine kinase and Ca^{2+} signals.
87 In addition, we identify CAMK2D and CAMK2G as novel downstream effectors of PEAK1 in
88 TNBC and 'repurposing' of the second generation CAMK2 inhibitor RA306 as a potential
89 therapeutic strategy against oncogenic PEAK1 signalling in poor prognosis human cancers

90 such as TNBC.

91

92 **Results**

93

94 *Characterization of dimer-specific interactomes of PEAK1 and PEAK2 by BiCAP*

95

96 To characterize the interactomes of PEAK1 and PEAK2 homodimers, and the PEAK1/PEAK2
97 heterodimer, we applied bimolecular complementation affinity purification coupled with
98 tandem mass spectrometry (BiCAP-MS/MS) (Supp. Fig. 1A)[22]. Specific dimeric complexes
99 were affinity purified and associated proteins identified by LC-MS/MS in data-independent
100 acquisition mode (Methods, Fig. 1A-C, Supp. Table 1). Strong correlation between triplicate
101 biological replicates was observed (mean sample correlation scores: Vector = 0.78; PEAK1
102 homodimer = 0.85; PEAK2 homodimer = 0.94; PEAK1/2 heterodimer = 0.94) (Supp. Fig.
103 1B). Grb2, a well-characterized PEAK1 binding partner[6, 16] bound the PEAK1 homodimer and
104 PEAK1/PEAK2 heterodimer, but not the PEAK2 homodimer, consistent with our previous
105 results that PEAK1 bridges Grb2 to PEAK2[16]. Two protein phosphatase 1 (PP1) family
106 members, PPP1CA and PPP1CC were previously identified as PEAK1 interactors in a
107 traditional immunoaffinity based-MS/MS screen[19]. However, their selectivity towards PEAK1
108 versus PEAK2 was unclear. Here, like Grb2, they were identified as interactors of the PEAK1
109 homodimer and PEAK1/PEAK2 heterodimer, with another PP1 family member, PPP1CB,
110 associating with the PEAK1 homodimer. Of interest given a recent paper reporting a key
111 regulatory role for 14-3-3 proteins in regulating PEAK3 effector recruitment and biological
112 activity[23], multiple 14-3-3 isoforms bound both homodimers and the heterodimer (Supp. Table
113 1). Further novel interactors identified included the RAC1 guanine nucleotide exchange factor
114 (GEF) FARP1 and the MAPK pathway antagonist SPRY4, which were selective for the

115 PEAK2 homodimer. In addition, Ca^{2+}/calmodulin-dependent protein kinase 2 (CAMK2)D and
116 G associated with the PEAK1 and PEAK2 homodimers and the PEAK1/PEAK2 heterodimer,
117 while CAMK2B was recruited by the PEAK2 homodimer and PEAK1/PEAK2 heterodimer
118 (Figs. 1A-C). Bioinformatic analysis of the interactomes for each of the PEAK complexes in
119 order to identify enriched pathways/processes identified calcium-related pathways that
120 included CAMK2 enzymes as being enriched (specifically 'postsynaptic signalling' for
121 PEAK1 and PEAK2 homotypic complexes and both 'myometrial' and 'cardiac signalling' for
122 all 3 complexes) (Supp. Table 2).
123 Overall, these data provided novel and important insights into the binding selectivity of
124 PEAK1/2 complexes and identified specific CAMK2 family members as novel interactors of
125 these pseudokinase scaffolds.
126
127 *Characterization of CAMK2 interaction with PEAK1 and PEAK2*
128
129 To confirm the association of specific CAMK2 family members with PEAK1 and PEAK2, we
130 focused on CAMK2D and CAMK2G, since these kinases associated with all of the homo- and
131 heterotypic PEAK complexes analysed by BiCAP-MS/MS. Interaction of these CAMK2s with
132 endogenous PEAK1 and PEAK2 was interrogated by proximity ligation assays in MDA-MB-
133 231 breast cancer cells (Fig. 1D-F). Using this technique, the interactions between PEAK1 and
134 CAMK2D or G could be detected and were significantly decreased when PEAK1 was knocked
135 down using siRNA (Fig. 1D-E). Similar results were observed for the interactions between
136 PEAK2 and CAMK2D or G (Fig. 1D,F). These data demonstrate that CAMK2D and G interact
137 with both PEAK1 and PEAK2 *in vivo,* at endogenous expression levels.
138
139 *Regulation of CAMK2 activity by PEAK1*

140

141 The known overexpression of PEAK1 in breast cancer[6, 7] led us to interrogate the functional
142 consequences of PEAK1/CAMK2 interaction. Upon an increase in intracellular Ca^{2+}, binding
143 of Ca^{2+}/calmodulin (CaM) to the CAMK2 regulatory segment leads to release of the regulatory
144 segment from the kinase domain, kinase activation, and phosphorylation of T286 (T287 in
145 CAMK2D and G). In the presence of T286 phosphorylation, the CAMK2 regulatory segment
146 can no longer mediate autoinhibition, and the activity of CAMK2 is Ca^{2+}/CaM autonomous [24].
147 Knockdown of PEAK1 in MDA-MB-231 TNBC cells did not affect the expression levels of
148 CAMK2D and G but significantly reduced their activation, as determined by phosphorylation
149 at T287 (Fig. 2A-B). In addition, overexpression of PEAK1 in these cells significantly
150 enhanced activation of these two CAMK2 isoforms (Fig. 2C-D). Positive regulation of
151 CAMK2D/G activity by PEAK1 was also observed in MDA-MB-468 TNBC cells (Supp. Fig.
152 2). Treatment of MDA-MB-231 cells with BAPTA/AM, a membrane permeable Ca^{2+} chelator
153 which blocks activation of CaM by Ca^{2+} [25] significantly reduced basal CAMK2 T287
154 phosphorylation and completely blocked the effect of PEAK1 on CAMK2 activation,
155 indicating that PEAK1-mediated CAMK2 activation is Ca^{2+}-dependent (Fig. 2E-F).
156

157 In light of this result, we determined whether PEAK1 can modulate Ca^{2+} levels and thereby
158 indirectly regulate CAMK2 activation. Application of Fluo-4 imaging revealed that PEAK1
159 overexpression significantly enhanced intracellular Ca^{2+} levels at steady state (Fig. 2G-H).
160 With regard to the mechanism underpinning PEAK1-regulated Ca^{2+} signalling, the known roles
161 of the PEAKs as regulators and/or substrates of specific tyrosine kinases[4, 5] led us to determine
162 whether PEAK1 overexpression impacts tyrosine phosphorylation and hence activation of
163 PLCγ1, leading to generation of IP_3 that triggers Ca^{2+} release from intracellular stores[26]. Indeed,
164 PEAK1 knockdown decreased tyrosine phosphorylation of PLCγ1 Y783 (Fig. 2I), while

165 PEAK1 overexpression enhanced PLCγ tyrosine phosphorylation on this site (Fig. 2J).
166 However, given that PEAK1 is a pseudokinase, PLCγ1 phosphorylation must be mediated by
167 a *bona fide* tyrosine kinase acting downstream of PEAK1. Since PEAK1 is a member of a
168 prominent Src family kinase (SFK) signalling network in TNBC[27] and PLCγ1 is a known
169 substrate of SFKs[28], we hypothesized that SFKs may mediate this role. Supporting this
170 hypothesis, treatment of MDA-MB-231 TNBC cells with the highly-selective SFK inhibitor
171 eCF506[29] blocked PEAK1-enhanced PLCγ1 tyrosine phosphorylation (Supp. Fig. 3).
172 However, interrogation of the BiCAP datasets did not reveal association of specific SFKs or
173 PLCγ1 with any of the PEAK complexes, strongly suggesting that the regulatory mechanism
174 does not involve direct binding.
175
176 *Structural requirements for PEAK1/2 interaction with CAMK2*
177
178 To determine which regions of PEAK1 and PEAK2 mediate interaction with CAMK2D and
179 G, we utilized previously described deletion mutants of PEAK1 and PEAK2[16] that delete the
180 N-terminal region (ΔN-term), N1 α-helix (ΔN1) and a combination of the pseudokinase
181 domain and helices J-M (ΔCterm), as well as a new mutant comprising just the extreme N-
182 terminal region (1-324 amino acids) (N-term) (Fig. 3A). Co-immunoprecipitation of Flag-
183 tagged PEAK1 with endogenous CAMK2D could be demonstrated for WT, ΔN1 and ΔCterm
184 PEAK1 but not for the ΔNterm PEAK1 mutant (Fig. 3B). However, the Nterm region alone
185 did not associate with CAMK2D, indicating that it is required but not sufficient for interaction
186 with these CAMK2s (Fig. 3B). In addition, since the N1 and Cterm regions are required for
187 PEAK1 to undergo homotypic association and also heterotypic interaction with PEAK2[16],
188 these data also indicated that dimerization is not required for PEAK1 to associate with these
189 CAMK2s. Next, we generated a series of deletion mutants to more narrowly define the

190 CAMK2 binding region on PEAK1 (Fig. 3C). Association with CAMK2D was lost with the
191 Δ261-324 mutant (Fig. 3D). Furthermore, deletion of smaller regions spanning amino acids
192 261-300 or 301-324 also abolished CAMK2D association (Fig. 3D). Deletion of amino acids
193 301-324 also markedly reduced CAMK2G association (Fig. 3E).
194
195 Although PEAK1 and PEAK2 share similar overall domain architecture, the N-terminal
196 extensions, including the region of PEAK1 required for CAMK2 association (amino acids 261-
197 324), are poorly conserved[16], indicating that the CAMK2 binding mechanism for PEAK2 is
198 likely to differ. Consistent with this hypothesis, while CAMK2D association with PEAK2 was
199 significantly reduced with the PEAK2 ΔNterm mutant, the greatest effect was observed with
200 the ΔN1 and ΔCterm mutants, which markedly and almost completely abolished association,
201 respectively (Supp. Fig. 4A-C). Since the N1 and Cterm regions are required for PEAK2 to
202 undergo homotypic and heterotypic association[16], these data suggest that PEAK2 interaction
203 with these CAMK2s requires PEAK2 dimerization. Supporting this model, three point
204 mutations in PEAK2 (Supp. Fig. 4A) that abrogate dimerization[18] all led to diminished
205 association with CAMK2D (Supp. Fig. 4D). This contrasts with PEAK1, where the
206 dimerization-impaired ΔN1 and ΔCterm mutants retained association with the CAMK2s. In
207 addition, PEAK1 knockdown did not disrupt association of PEAK2 with CAMK2D (Supp. Fig.
208 4E), indicating that PEAK2 interaction with CAMK2D is not mediated via PEAK1, consistent
209 with the BiCAP data (Fig. 1B). Taken together, these data highlight contrasting structural
210 requirements for PEAK1 and PEAK2 association with CAMK2, with a greater contribution
211 from a discrete N-terminal region in the case of PEAK1, and a requirement for dimerization in
212 the case of PEAK2.
213

214 *PEAK1 directly binds CAMK2 via a conserved motif to promote CAMK2 activation and*
215 *PEAK1 phosphorylation*
216
217 Since the PEAK1 Δ301-324 mutant was deficient in CAMK2 association (Fig. 3D-E), we
218 determined the effect of this mutant on CAMK2 activation. Interestingly, this mutant was
219 significantly impaired in its ability to activate CAMK2D/G as determined by phosphorylation
220 at T287 (Fig 3F-G), indicating that PEAK1-mediated CAMK2 activation requires association
221 of the two proteins in addition to a Ca^{2+} signal (Fig. 2E-F).
222
223 A recent report characterized how CAMK2 interacts with substrate binding partners via a
224 conserved sequence motif in the binding partner, R/K-X-X-ϕ-X-R/K-X-X-S/T-ϕ (where ϕ
225 represents a hydrophobic residue) that binds across a single continuous site on the CAMK2
226 kinase domain[30]. It also revealed that binding of the conserved CAMK2 interaction motif
227 (CIM) competes with autoinhibition of CAMK2 by the regulatory segment of the kinase
228 domain, explaining the ability of certain substrates, such as GluN2B, to lock CAMK2 in an
229 active conformation[30]. Of note, the Rac GDP/GTP exchange factor TIAM1 exhibits a
230 pseudosubstrate version of the conserved motif (with A rather than S/T), but is still able to bind
231 and promote phosphorylation of itself on other sites[31]. To address whether PEAK1 may interact
232 with CAMK2 via this mechanism, we searched the PEAK1 N-terminal region for the conserved
233 motif. We first constructed a multiple sequence alignment across diverse species and
234 subsequently subjected this to MEME analysis to identify conserved motifs. This analysis
235 revealed that the PEAK1 amino acids 297-307 exhibit close similarity to the canonical binding
236 motif but with an alanine at position 0 (amino acid 306), as observed with TIAM1 (Fig. 4A).
237 Furthermore, the N-terminal region and the binding motif are highly conserved across species
238 (Supp. Fig. 5).

239

240 The presence of a CIM between amino acids 297-307 is consistent with disruption of binding
241 by deletion of amino acids 261-300 and 301-324 (Fig. 3D-E) and the failure of the Δ301-324
242 mutant to activate CAMK2 (Fig 3F-G). To determine whether a synthetic peptide
243 corresponding to the PEAK1 CIM bound CAMK2, we applied isothermal calorimetry. These
244 data revealed a high affinity interaction with a mean dissociation constant (K_D) of 635 nM (Fig.
245 4B), comparable to that of the TIAM1 interacting region (1.1 μM)[30]. Modelling of the
246 PEAK1/CAMK2 interaction using AlphaFold predicts (pLDDT 90.7, pTM 0.899) that the
247 PEAK1 CIM interacts across the same surface of the CAMK2 kinase domain as other known
248 interactors[30], with key salt bridges formed between PEAK1 R303 (-3 position) and R297 (-9)
249 with glutamate residues in CAMK2 (Fig. 4C-F, Supp. Fig. 6). In addition, L301 is
250 accommodated in a hydrophobic pocket of CAMK2 (Fig. 4E). We also note the predicted
251 formation of salt bridges and electrostatic interactions by PEAK1 D308, D310, D311 and D314
252 across the surface of CAMK2 (Fig. 4F). Of note, while this modelling was undertaken with
253 CAMK2A, the binding site is conserved across all CAMK2 isoforms, as highlighted by
254 AlphaFold2 modelling and multiple sequence alignments of CAMK2A, B, D and G (Supp.
255 Fig. 6).

256

257 To test the importance of key residues within the PEAK1 CIM for CAMK2 activation, we
258 generated PEAK1 mutants with alanine substitutions at the R303 (-3), L301 (-5) and R297 (-
259 9) positions (termed AAA) and glutamate substitutions at R303 and R297 (EE).
260 Overexpression of these two mutants significantly enhanced intracellular Ca^{2+} levels (Fig. 5A-
261 B) and PLCγ1 tyrosine phosphorylation (Fig. 5C-D). However, the mutants lost the ability to
262 activate CAMK2 as determined by phosphorylation at T287 (Fig. 5E-G). These data indicate
263 that while the ability of PEAK1 to activate CAMK2 is calcium-dependent (Fig. 2E-F), PEAK1-

264 enhanced Ca^{2+} is not sufficient to increase CAMK2 T287 phosphorylation, and direct
265 association with CAMK2 is also required. The data also support the validity of the Alphafold
266 modelling.
267
268 CAMK2 binding to TIAM1 leads to sustained phosphorylation of TIAM1[31]. To determine
269 whether PEAK1 is a substrate for CAMK2, we utilized RA306, a 'next generation' CAMK2
270 inhibitor developed by Sanofi for chronic cardiovascular indications that is selective for
271 CAMK2D and G over other isoforms[32]. RA306 exhibited 'on-target' activity against CAMK2
272 in MDA-MB-231 cells (Supp. Fig. 7A) and significantly inhibited PEAK1 serine/threonine
273 phosphorylation (Fig. 6A-B). In addition, recombinant CAMK2 demonstrated *in vitro* kinase
274 activity towards PEAK1 that was detectable using a pAkt substrate antibody that also
275 recognizes the minimal CAMK2 consensus motif for phosphorylation (RXXS/T) or a pSer/Thr
276 antibody (Fig. 6C). Interestingly, PEAK1 phosphorylation was markedly reduced when the
277 PEAK1 AAA and EE CIM mutants were used as substrate, indicating that efficient
278 phosphorylation of PEAK1 by CAMK2 requires interaction of the two proteins via the PEAK1
279 CIM (Fig. 6C).
280
281 *CAMK2 phosphorylates PEAK1 to regulate the PEAK1 interactome*
282
283 In order to characterize the impact of CAMK2-mediated phosphorylation on PEAK1
284 scaffolding potential, we compared the interactomes of wild-type (WT) PEAK1 and the AAA
285 and EE CIM mutants *in vivo*. We utilized this approach since it more selectively addresses the
286 impact of CAMK2-mediated PEAK1 phosphorylation, while RA306 treatment would exert a
287 more general inhibition of CAMK2-mediated cellular phosphorylation. Binding of the adaptors
288 Crk-L and Grb2, which associate with PEAK1 via SH3 and SH2 domain-mediated interactions,

289 respectively[23,9], was unaffected by the CIM mutations (Supp. Fig. 7B). In contrast, Western
290 blotting of PEAK1 IPs revealed significantly reduced association of 14-3-3 proteins with the
291 two mutants (Supp. Fig. 7C-D). Since 14-3-3 binding to client proteins is classically
292 phosphorylation-dependent, this indicated that impaired CAMK2 activation by the CIM
293 mutants leads to decreased phosphorylation of PEAK1 on 14-3-3 binding sites. Next, we
294 assayed heterotypic association of PEAK1 with PEAK2, a critical determinant of signal output,
295 with PEAK2 binding being required for PEAK1 to promote cell migration and oncogenic
296 signalling[16]. Importantly, whereas heterotypic association of wildtype PEAK1 with PEAK2 in
297 MDA-MB-231 TNBC cells could be readily detected, this was markedly reduced for the CIM
298 mutants (Figure 6D). Overall, these data demonstrate that CAMK2-mediated PEAK1
299 phosphorylation is a critical regulator of PEAK1-mediated protein-protein interactions and
300 signalling.
301
302 *PEAK1/CAMK2 signalling is a therapeutically 'actionable' target in TNBC*
303
304 The finding that CAMK2 and PEAK1 reciprocally regulate led us to interrogate how
305 expression of these proteins is related to breast cancer patient survival. Interestingly, combined
306 high expression of PEAK1 and CAMK2D was significantly associated with poor overall
307 survival, while a non-significant trend was detected for the PEAK1/CAMK2G combination
308 (Supp. Fig. 8A-C). Of note, this analysis emphasized the importance of high expression of both
309 PEAK1 and CAMK2D (Supp. Fig. 8B), consistent with a co-activating PEAK1/CAMK2D
310 'cassette' promoting breast cancer progression. To gain further insights into the combined role
311 of PEAK1 and CAMK2/G in breast cancer, we interrogated their association with distant
312 metastasis-free survival (DMFS). However, this was only possible with a meta-cohort derived
313 from certain publicly-available datasets (see Methods) and for the PEAK1/CAMK2G

314 combination. Nevertheless, this revealed a significant association between high
315 PEAK1/CAMK2G and reduced DMFS (Supp. Fig. 8D).
316
317 Next, we characterized the effects of PEAK1/CAMK2 signalling on biological endpoints in
318 TNBC cells. Previously we reported that CRISPR-mediated PEAK1 KO in MDA-MB-231
319 cells significantly reduced anchorage-dependent proliferation as well as tumoursphere
320 formation in low attachment plates[8]. Interestingly, treatment with RA306 resulted in a dose-
321 dependent reduction in viability of these cells under anchorage-dependent and -independent
322 conditions (high and low attachment plates, respectively) (Supp. Fig. 9A-B). These effects
323 appeared to be mediated via decreased proliferation, as PEAK1 KO or RA306 did not induce
324 apoptosis (Supp. Fig. 9C-D). Taken together, these data indicate that both PEAK1 and CAMK2
325 contribute to proliferative signalling in TNBC.
326 Next, we probed the role of PEAK1/CAMK2 in cell migration/invasion. Knockdown of either
327 CAMK2D or G blocked the effect of PEAK1 overexpression on cell migration and invasion
328 (Fig. 7A-B, Supp. Fig. 10A) and RA306 treatment blocked PEAK1-promoted migration in
329 both MDA-MB-231 and -468 cells (Fig. 7C, Supp. Fig. 10B-C) and PEAK1-promoted invasion
330 in MDA-MB-231 cells (Supp. Fig. 10D). Furthermore, the Δ301-324 PEAK1 mutant, which
331 cannot bind or activate CAMK2 (Fig. 3D-G), was unable to enhance TNBC cell migration and
332 invasion (Fig. 7D, Supp. Fig. 10E). Overall, these data indicate a requirement for CAMK2
333 expression and/or activation, as well as PEAK1/CAMK2 binding, in regulation of cell
334 migration and invasion by PEAK1.
335
336 We then evaluated RA306 in an *in vivo* model of TNBC tumour growth and metastasis.
337 Previously, we demonstrated that PEAK1 gene knock-out significantly inhibited growth and
338 lung metastasis of orthotopic MDA-MB-231 TNBC xenografts[8]. To test RA306, we utilized

339 the highly metastatic variant of this cell line, MDA-MB-231-HM[33], so that we could readily
340 assay metastatic spread from the primary tumour. In addition, we generated PEAK1-deficient
341 MDA-MB-231-HM cells via CRISPR editing (Supp. Fig. 11A) to compare the effect of RA306
342 with PEAK1 knock-out and also the combined effect of these two manipulations. On target
343 activity of RA306 could be detected in the xenografts and PEAK1 ablation also reduced
344 CAMK2 activation (Supp. Fig. 11B-C). RA306 treatment significantly impaired primary
345 tumour growth (Fig. 7E). Importantly, the degree of growth inhibition was similar to that
346 observed upon PEAK1 gene knock-out and combining RA306 with gene knock-out did not
347 enhance this further, strongly suggesting that RA306 treatment and PEAK1 knock-out are
348 targeting the same oncogenic signalling axis (Fig. 7E). Furthermore, we also allowed a separate
349 cohort of primary tumours to grow to the same mean size (Supp Fig 11D), resected them and
350 then monitored metastasis. Strikingly, RA306 blocked metastasis to a similar extent to PEAK1
351 knock-out (Fig 7F). Since PEAK1 KO or RA306 treatment impacts cell proliferation, migration
352 and invasion but not apoptosis[8] (Fig. 7, Supp. Fig. 9-10), the effect on primary tumour growth
353 is likely mediated via reduced proliferation while the reduced metastatic growth must be
354 independent of primary tumour size and reflect a decreased ability to metastasize to the lung
355 and/or reduced proliferation at this secondary site. Overall, these data identify RA306 as a
356 potential therapeutic strategy against the PEAK1/CAMK2 axis in TNBC and potentially other
357 human cancers.
358
359 **Discussion**
360
361 The pseudokinase scaffold PEAK1 has emerged as a critical regulator of intracellular
362 signalling, transducing and integrating pleiotropic signals downstream of a variety of growth
363 factor receptors and integrins. For example, PEAK1 promotes Ras activation via Grb2

364 binding[6], and couples to paxillin regulation at focal adhesions via Crk[8]. In addition, it can
365 indirectly impact Csk and Stat3 via association with PEAK2[16] and ASAP1, PYK2 and Cbl via
366 PEAK3[4]. Our discovery that PEAK1 can also promote Ca^{2+} signals via PLCγ1 and moreover,
367 binds and sustains activation of the Ca^{2+} effector CAMK2 greatly expands the signalling
368 repertoire of this scaffold and cements its role as a fundamental cell signalling nexus. It also
369 identifies PEAK1 as the first member of the kinase superfamily to sustain activation of
370 CAMK2 via direct binding and the first oncoprotein to target CAMK2 via this mechanism.
371 This expansion of the known signalling functions of PEAK1 calls for a re-evaluation of its role
372 in physiological processes linked to CAMK2 signalling including learning and memory,
373 cardiac function and osteogenic differentiation[20]. As discussed later, it also highlights a
374 potential strategy for therapeutically targeting the oncogenic activity of PEAK1.
375
376 Our findings lead to a model whereby PEAK1 enhances and prolongs CAMK2 activation and
377 signalling by two mechanisms that together provide a 'feed-forward' regulatory process for
378 CAMK2 (Figure 8). First, PEAK1 overexpression leads to enhanced and more sustained Ca^{2+}
379 signals in cells, reflecting increased tyrosine phosphorylation and hence activation of PLCγ1
380 which is driven in a SFK-dependent manner. While the role of SFKs in this pathway is
381 consistent with PEAK1 functioning within a SFK signalling network in TNBC[27], the detailed
382 mechanism currently remains unclear, and based on our BiCAP data, does not appear to involve
383 direct binding of PEAK1/2 to SFKs or PLCγ1. In this regard, it differs from the direct binding
384 and regulation of the tyrosine kinases Csk and PYK2 by PEAK2 and PEAK3, respectively[12,
385 34]. In terms of the SFKs responsible, TNBCs express several SFKs including Src, Yes, Fyn and
386 Lyn, but expression of the latter is particularly high, and since Lyn also regulates PEAK1
387 tyrosine phosphorylation, it represents an interesting candidate for further investigation[6, 27, 35].
388 The enhanced Ca^{2+} signal generated by this PEAK1/SFK/PLCγ1/Ca^{2+} pathway leads to a

389 greater pool of activated CAMK2. Second, PEAK1 binds directly to the Ca^{2+}-activated
390 CAMK2 via the conserved CIM and this has two effects – first, it leads to sustained CAMK2
391 activation, as determined by T287 phosphorylation, and second, it promotes CAMK2-mediated
392 PEAK1 phosphorylation.
393
394 Promotion of CAMK2 T287 phosphorylation and PEAK1 phosphorylation by binding of the
395 PEAK1 CIM to CAMK2 can be explained by a model that incorporates two key characteristics
396 of this enzyme/interactor system - first, the known ability of CAMK2 to form a large
397 holoenzyme comprising 12-14 monomers [24] and second, PEAK1 CIM binding 'locking'
398 CAMK2 in an active state with the αD helix rotated outward[30] (Figure 8). In this model,
399 repeated cycles of association/disassociation of one PEAK1 CIM to different CAMK2 subunits
400 within the complex leads to sustained activation of a subset of subunits, allowing continued
401 autophosphorylation on T287, which occurs *in trans* [24]and phosphorylation of PEAK1.
402 However, we accept that alternative, or contributory, mechanisms are conformational changes
403 within the holoenzyme induced by PEAK1 binding to one monomer that promote more
404 widespread enzyme activation and autophosphorylation, and T287 being protected from
405 phosphatase action by PEAK1 binding to CAMK2. In addition, CIM-mediated recruitment of
406 PEAK1 to one monomer within the Ca^{2+}-activated oligomer leads to phosphorylation of
407 PEAK1 by other activated monomers within the complex. This would be facilitated by the
408 relatively large number of consensus CAMK2 phosphorylation sites present on PEAK1 (41
409 R/KXXS/T sites in total). Importantly, a precedent for a reciprocally-activating interaction of
410 CAMK2 with a binding partner exhibiting a pseudosubstrate CIM is provided by
411 CAMK2/TIAM1. Here, binding of the TIAM1 CIM to CAMK2 leads to sustained
412 phosphorylation of TIAM1 by CAMK2[31].
413

414 An interesting question is the stoichiometry of the resulting PEAK1/CAMK2 complexes.
415 While CAMK2 forms a large holoenzyme complex of 12-14 subunits, PEAK1 can form dimers
416 via the SHED domain and also higher order oligomers via pseudokinase domain interfaces[18].
417 These properties may facilitate formation of assemblies with CAMK2 oligomers. In addition,
418 the localization of the PEAK1 CIM towards the N-terminus of a largely disordered extension
419 provides considerable flexibility for assembly of large multimeric protein complexes.
420 Interestingly, in contrast to PEAK1, PEAK2 lacks a consensus CIM, and its dimerization
421 potential is essential for CAMK2 association. While the impact of PEAK2 on CAMK2
422 regulation requires further characterization, one possibility is that PEAK2 contributes to
423 assembly of higher-order complexes of PEAK1/2 with CAMK2.
424
425 While PEAK1 is known to be regulated by site-selective tyrosine phosphorylation[6, 19, 36], our
426 study provides the first demonstration of positive regulation of PEAK1 by serine/threonine
427 phosphorylation. Furthermore, we determine that like tyrosine phosphorylation, this regulates
428 the PEAK1 interactome. In particular, the two PEAK1 CIM mutants, which are poor substrates
429 for CAMK2, exhibit decreased association with PEAK2. This provides one explanation for the
430 role of CAMK2 in PEAK1-enhanced migration, since heterotypic interaction with PEAK2 is
431 required for this process[16]. Conceivably, CAMK2-mediated phosphorylation may regulate
432 PEAK1 conformation and accessibility of the dimerization and/or oligomerization interfaces.
433 Another protein that exhibits significantly reduced binding to the PEAK1 CIM mutants is 14-
434 3-3. This is consistent with the overlap between the minimal CAMK2 phosphorylation site
435 consensus (R/KXXS/T) and the 14-3-3 mode 1 motif for binding, RXXpS/TXP. In the case of
436 PEAK3, 14-3-3 binding to phosphorylated PEAK3 S69 impairs Grb2 and Crk recruitment to
437 the scaffold, and the PEAK3 S69A mutant exhibits markedly enhanced ability to promote cell
438 migration[23]. With PEAK1, the overall effect of CAMK2-mediated phosphorylation on PEAK1-

439 promoted migration/invasion is positive, so 14-3-3 binding may downregulate binding of
440 negative regulatory factors, and/or increase association with positive ones, such as PEAK2.
441
442 Reflecting their role in a variety of disease states, pseudokinases have emerged as potential
443 therapeutic targets, albeit challenging ones given their lack of catalytic activity. Possible
444 therapeutic intervention strategies include the use of small molecule allosteric regulators,
445 therapeutic antibodies for cell surface receptor pseudokinases such as HER3, targeted
446 degradation approaches eg using PROTACs, and pharmacologic modulation of 'actionable'
447 downstream effector pathways[3]. The oncogenic pseudokinase PEAK1 presents a particular
448 conundrum, since it does not bind ATP or GTP, the dimerization interface is relatively large
449 and difficult to target using small molecule drugs, and PEAK1 is an intracellular protein and
450 therefore not accessible by standard therapeutic antibody approaches[5]. However, in this study
451 we identify a novel strategy for targeting PEAK1 signalling that exploits the functional
452 dependency of this kinase on a readily 'actionable' *bona fide* kinase, CAMK2. Importantly,
453 supporting therapeutic targeting of this serine/threonine kinase, CAMK2 isoforms are
454 overexpressed in a variety of human cancers, including breast cancer, where they promote cell
455 proliferation, migration and invasion[20, 21]. They are also positively associated with metastasis.
456 In an animal model of prostate cancer metastasis, genetic ablation of all CAMK2 family
457 members significantly reduced lymph node metastasis[37]. Expression, as well as activation, of
458 CAMK2 is significantly higher in lymph node metastases than primary breast cancers, and high
459 expression of the CAMK2 family is associated with worse DMFS in TNBC[21]. In addition, brain
460 metastatic colonization of TNBC is associated with CAMK2 signaling[38]. Our work now
461 provides novel insights into the oncogenic mechanism of CAMK2, with a key role being
462 CAMK2-mediated phosphorylation of PEAK1. This promotes heterodimerization of PEAK1
463 with PEAK2, a process required for PEAK1 to promote cell migration, presumably because

464 PEAK2 recruits/activates critical effectors such as Csk and Stat3 [16]. In addition, the activated
465 CAMK2 may phosphorylate other downstream targets that promote metastasis, such as the Rho
466 family GEF TIAM1 [31], and regulate the focal adhesion proteins FAK and paxillin[39].
467 In general, characterization of the oncogenic role of CAMK2 has been compromised by a poor
468 understanding of regulatory mechanisms, with functional studies often utilizing constitutively
469 active mutants, as well as a reliance on tool compounds for CAMK2 inhibition, such as KN93,
470 that have numerous off-target effects[40]. Our study addresses these issues by identifying the
471 oncogenic pseudokinase PEAK1 as a novel feed-forward activator of CAMK2 and the second
472 generation CAMK2D/G inhibitor RA306 as a suitable targeted agent to block PEAK1/CAMK2
473 signalling in TNBC and other cancers where PEAK1 is involved, such as pancreatic cancer.
474 Importantly, RA306 avoids central nervous system side-effects and exhibits good oral
475 bioavailability, highlighting its potential for oncology re-purposing[32]. In addition, the
476 identification of a reciprocally-activating PEAK1/CAMK2 complex indicates that these two
477 proteins could be used as predictive biomarkers to guide patient stratification for anti-CAMK2
478 treatment. Overall, our work identifies an unsuspected interaction across the kinase superfamily
479 with significant implications for our understanding of cell signalling in normal and disease
480 states and precision targeting of PEAK1 and CAMK2.
481
482 **Methods**
483 *Plasmids and siRNAs*
484 The retroviral expression vector pRetroX-IRES-DsRedExpress (DsR) containing N-terminal
485 HA-tagged and C-terminal FLAG/Myc-tagged PEAK1 as well as its deletion mutants
486 including ΔNterm, ΔCterm and ΔN1, together with the expression vector pMIG containing N-
487 terminal HA-tagged and C-terminal FLAG-tagged PEAK2 as well as PEAK2 site mutants
488 (L955A, L966A, W1382A) were previously generated in our laboratory[16, 18]. pRetroX-IRES-

489 DsRedExpress plasmid containing Flag-tagged PEAK1 N terminal (residues 1–324) deleted
490 and other mutants (Δ1-260, Δ261-300, Δ261-324, Δ301-324, R297A/L301A/R303A and
491 R297E/R303E) were purchased from GenScript.
492 pDEST-V1 (Addgene plasmid 73637) and pDEST-V2 (Addgene plasmid 73638) vectors were
493 assembled from various recombinant and synthetic components as described previously[22].
494 Vectors expressing V1- or V2-labeled fusions of PEAK1 or PEAK2 were generated by
495 recombination cloning from pDONR223-PEAK1 and pDONR223-PEAK2 constructs into
496 pDEST-V1 or pDEST-V2 destination vectors using Gateway LR Clonase enzyme mix (Life
497 Technologies) according to the manufacturer's instructions and verified by sequencing. The
498 expression vector encoding full-length Venus fluorescent protein was a gift from S. Michnick
499 (University of Montreal).
500 CAMK2A kinase domain (residues 7-274) was cloned into a pET vector containing an N-
501 terminal 6×His followed by a SUMO tag. A D135N mutation was introduced by site-directed
502 mutagenesis.
503 Sequences of siRNAs were PEAK1 (ON-TARGETplus Human PEAK1 siRNA, cat. LQ-
504 005339-00-0010), PEAK2 (MISSION Human PEAK2 siRNAs, cat. #1:
505 SASI_Hs02_00316033, #2: SASI_Hs02_00316034, #3: SASI_Hs02_00316035, #4:
506 SASI_Hs02_00316036), CAMK2D (siGENOME Human CAMK2D siRNAs, cat. #1: D-
507 004042-02-0002, #2: D-004042-03-0002, #3: D-004042-04-0002, #4: D-004042-05-0002),
508 CAMK2G (siGENOME Human CAMK2G siRNAs, cat. #1: D-004536-01-0005, #2: D-
509 004536-03-0005, #3: D-004536-05-0005, #4: D-004536-06-0005). Negative control siRNA
510 was ON-TARGET plus Non-targeting pool (Dharmacon, D-001810-10-20).
511
512 *Antibodies*

513 The following antibodies were purchased from Santa Cruz Biotechnology (Dallas, TX):
514 PEAK1 (cat. sc-100403), β-actin (cat. sc-69879) and Pan 14-3-3 (cat. sc-1657). CAMK2D (cat.
515 ab181052) and CAMK2G (cat. ab201966) were purchased from Abcam. Phospho-Akt
516 Substrate (RXXS*/T*) (cat. 9614), T-CAMK2 (cat. 4436), CAMK2-pT287 (cat. 12716), PLC-
517 γ (cat. 5690S), PLC-γ-pY783 (cat.14008S) and cleaved PARP Asp 214 (cat. 9546) were
518 purchased from Cell Signaling Technology. Flag (cat. F1804 and F7425), and α-tubulin (cat.
519 T5168) were purchased from Sigma. The following antibodies were also used: CAMK2D
520 (Genetex, cat. GTX111401), HA (Roche Applied Science, cat. 11867423001). Phospho-
521 Ser/Thr antibody (cat. 612548) was purchased from BD Transduction Laboratories. The
522 custom-made PEAK2 (SgK223) antibody was generated by Cambridge Research
523 Biochemicals Ltd. by standard procedures and described previously[14].
524
525 *Inhibitors and chemicals*
526 RA306 was custom synthesized by Reagency (cat. RGNCY-0117). The SFK inhibitor eCF506
527 was obtained from Professor Margaret Frame (Edinburgh Cancer Research Centre). Captisol
528 (cat. A508148) was purchased from AmBeed. BAPTA-AM (cat. A1076) and DMSO (cat.
529 d8418) were purchased from Sigma. Doxorubicin-HCl was obtained from Selleckchem (cat.
530 S1208).
531
532 *Cell lines and Tissue Culture*
533 HEK293T cells were maintained in Dulbecco's Modified Eagle's Medium (DMEM, Gibco,
534 cat. 1200046) supplemented with 10% (v/v) fetal bovine serum (FBS; Fisher Biotech, cat. S-
535 FBS-US-015). MDA-MB-231 parental cells were obtained from EG&G Mason Research
536 Institute, Worcester, MA. MDA-MB-231 cells stably expressing the murine ecotropic receptor
537 (MDA-MB-231_EcoR) were a kind gift from A/Prof Maija Kohonen-Corish at the Garvan

538 Institute of Medical Research. MDA-MB-468 cells were obtained from the American Type
539 Culture Collection (ATCC). The highly metastatic MDA-MB-231 cell line (MDA-MB-
540 231_HM) was originally established by Prof. Zhou Ou from Fudan University Shanghai Cancer
541 Center in China. The MDA-MB-231_HM cell line expressing luciferase/mCherry was a kind
542 gift from A/Prof. Erica Sloan at Monash University. In this paper, MDA-MB-231_HM refers
543 to the cell line expressing luciferase/mCherry.
544 Breast cancer cell lines were maintained in RPMI-1640 medium (Life Technologies, cat.
545 11875119 and Gibco, cat. 31800-089) supplemented with 10% FBS (Fisher Biotec, cat. S-FBS-
546 US-015), 10 μg/mL Actrapid penfill insulin (Clifford Hallam Healthcare), and 20 mM HEPES
547 (Life Technologies, cat. 15630080). All cell lines were authenticated by short tandem repeat
548 polymorphism, single-nucleotide polymorphism, fingerprint analyses and underwent routine
549 mycoplasma testing by PCR.
550
551 *Cell Lysis, Immunoprecipitation, and Immunoblotting*
552 Cell lysates for immunoblotting and immunoprecipitation (IP) were prepared using
553 radioimmunoprecipitation (RIPA) buffer and normal lysis buffer (NLB), respectively[41]. For IP
554 of overexpressed Flag- or HA-tagged proteins, cell lysates were incubated with either anti-
555 FLAG M2 affinity-agarose beads (Sigma, cat. A2220) or red anti-HA affinity gel (Sigma, cat.
556 E6779) at 4°C for 2 - 4 h with end-to-end rotation. After the incubation, the beads were washed
557 extensively with ice-cold lysis buffer, the immune complexes were eluted with SDS-PAGE
558 loading buffer, and subjected to Western blotting analysis, which was performed following
559 SDS-polyacrylamide gel electrophoresis using 5% stacking gels and 8%, 10% or 12%
560 separating gels. In order to ensure that phospho and total antibodies were used at non-limiting
561 concentrations, Western blot analyses were undertaken on dilution series of cell lysates.
562

563 *Generation of PEAK1 knock-out cells*

564 Stable MDA-MB-231_HM PEAK1 knockout cells were generated using the Synthego
565 Immortalized Cell Nucleofection Protocol as per manufacturer's instructions (Synthego).
566 Briefly, ribonucleoprotein (RNP) complexes were assembled by combining Cas9 2NLS
567 (Synthego), human PEAK1 sgRNA (Gene Knockout Kit v2, Synthego) and Nucleofector
568 SolutionTM L + supplement (Synthego) and incubating at room temperature for 10 mins. RNP
569 complexes were combined with cells in NucleocuvetteTM strips immediately prior to
570 electroporation. Cells were electroporated using the 4D-X Core unit (Lonza) using setting CH-
571 125. Cells were immediately resuspended in normal culture medium following electroporation.
572 Cell lysates were collected 72h post-electroporation to confirm PEAK1 knockout efficiency by
573 Western blot.

574

575 *Transfections*

576 SMARTpool siRNA or individual siRNA duplexes were applied to cells using DharmaFECT
577 (Dharmacon, Lafayette, CO) transfection reagent according to the manufacturer's instructions.
578 Plasmid transfections were performed using Lipofectamine 3000 (Invitrogen) according to the
579 manufacturer's instructions.

580

581 *BiCAP purification*

582 This was performed as previously described[22]. Briefly, HEK293T cells were transfected with
583 the appropriate BiCAP constructs. Cells were lysed with ice-cold lysis buffer comprising 50
584 mM Tris (pH 7.4), 150 mM NaCl, 1 mM EDTA, 1% (v/v) TritonX-100 supplemented with
585 fresh EDTA-free protease inhibitor cocktail and 0.2 mM sodium orthovanadate. Samples were
586 cleared by centrifugation at 18,000 g for 10 min at 4 °C to remove cellular debris. Total protein
587 concentration was determined by Bradford assay using Bio-Rad Protein Assay Dye Reagent

588 Concentrate (Bio-Rad Laboratories) according to the manufacturer's instructions. To purify
589 BiCAP dimers (or Venus alone as a negative control for nonspecific interactions), 1 mg of total
590 lysate was incubated with 35 µl of GFP-Trap_A agarose beads slurry (ChromoTek GmbH) for
591 2 h at 4°C with end-to-end rotation. Beads were extensively washed with wash buffer [10 mM
592 Tris (pH 7.5), 150 mM NaCl, 0.5 mM EDTA] and subjected to on-bead digestion with trypsin,
593 and the resulting peptides were analyzed by mass spectrometry (MS). Samples from each
594 experimental condition were subjected to data-dependent acquisition (DDA) to construct a
595 spectral library. Three biological replicates for each condition were then analysed by data-
596 independent acquisition (DIA) to characterize the corresponding interactomes. Conditions for
597 DDA and DIA are detailed below.
598
599 *Mass spectrometry-based proteome analysis*
600 MS analysis was based on an UltiMate 3000 RSLC nano-LC system (Thermo Fisher Scientific)
601 coupled to a Q Exactive Plus Mass Spectrometer (Thermo Fisher Scientific). The peptides were
602 loaded via a Pepmap100 trap column, 100 µm × 2 cm nanoviper, (Thermo Fisher Scientific),
603 eluted and separated on a Pepmap100 RSLC analytical column, 75 µm × 50 cm, nanoViper,
604 C18 (Thermo Fisher Scientific). For each injection, 1 µg of peptides was loaded onto the
605 column and eluted using increasing concentrations of buffer B (80% acetonitrile / 0.1% formic
606 acid) at 250 nL/min over 150 min. The eluent was nebulized and ionized using a
607 nanoelectrospray source (ThermoFisher Scientific) with a distal-coated fused silica emitter
608 (Trajan, Ringwood, Victoria, Australia). The capillary voltage was set at 1.7 kV.
609 To generate spectral libraries for proteomics, the MS was firstly operated in DDA mode to
610 automatically switch between full MS scans and tandem MS/MS scans. Survey full scan MS
611 spectra (m/z 375–1700) were acquired in the Orbitrap with 70 000 resolution after
612 accumulation of ions to a 1×10^6 target value with a maximum injection time of 120 ms. Up to

613 12 of the most intensely charged ions (z ≥ +2) were sequentially isolated and fragmented in the
614 collision cell by higher-energy collisional dissociation with the following parameters, fixed
615 injection time of 120 ms, 35 000 resolution and automatic gain control target of 5×10^5.
616 Dynamic exclusion was set to 15 s.
617 The DIA mode consisted of a MS1 scan (scan range from 400 to 1220 m/z, at resolution of
618 35 000, an AGC target of 5×10^6 and a maximum ion injection time of 120 ms) followed by
619 MS2 scans with 60 DIA windows at a resolution of 35 000, an AGC target of 3×10^6 with
620 automatic injection time, isolation window of 30 m/z. The stepped collision energies were
621 22.5%, 25%, and 27.5%. The spectra were recorded in profile type.
622
623 *Data Processing*
624 The DDA spectra were analyzed with MaxQuant (version 1.5.2.8) [42] against the human UniProt
625 fasta database (v2015–08, 20,210 entries) using default settings. The spectral library was then
626 generated in Spectronaut® software (version 8, Biognosys, Schlieren, Switzerland) and
627 normalized to iRT peptides. The DIA data were firstly transformed into htrms format and
628 analyzed with Spectronaut® using default settings. The MS data were searched against the same
629 human UniProt database and the aforementioned spectral library. The false discovery rate
630 (FDR) was set to 1% at peptide and protein level. Perseus (version 2019) was used to normalize
631 the data and impute for missing values [43]. Candidate interacting proteins were defined by
632 applying the following criteria: p value <0.05 by two-tailed *t*-test and a log2 fold change of ≥
633 1.5 against the Venus control. Pathway enrichment was undertaken using the WikiPathways
634 Database.
635
636 *Protein expression and purification*
637 CAMK2A D135N kinase domain was recombinantly expressed in BL21(DE3) cells

638 (Millipore) as previously described[30]. Protein expression was induced for ~6 h by 1 mM
639 isopropyl β-a-D-1-thiogalactopyranoside (IPTG; GoldBio) in an 18 ºC shaker. Cell pellets were
640 resuspended and lysed in Buffer A [25 mM Tris pH 8.5, 50 mM KCl, 40 mM imidazole, 10%
641 glycerol] with protease inhibitor mixture [0.2 mM AEBSF, 5.0 μM leupeptin, 1 μg/ml
642 pepstatin, 1 μg/ml aprotinin, 0.1 mg/ml trypsin inhibitor, 0.5 mM benzamidine] and DNase (1
643 μg/ml; Sigma). Protein purification was performed using an ÄKTA pure chromatography
644 system at 4 °C. After pelleting the cell debris, clarified cell lysate was loaded onto two 5 mL
645 HisTrap FF Ni-NTA Sepharose columns (GE) and eluted with a combination of 50% buffer A
646 and 50% buffer B [25 mM Tris-HCl pH 8.5, 150 mM KCl, 1 M imidazole, 10% glycerol] for
647 a final concentration of 0.5 M imidazole. Protein was desalted using a HiPrep 26/10 desalting
648 column (GE), and His-SUMO tags were cleaved with Ulp1 protease overnight at 4 °C in buffer
649 C [25 mM Tris-HCl pH 8.5, 40 mM KCl, 40 mM imidazole, 2 mM tris(2-carboxyethyl)
650 phosphine (TCEP), 10% glycerol]. Cleaved tags were separated by a subtractive Ni-NTA step
651 followed by an anion exchange step performed with a 5-ml HiTrap Q-FF (GE) and protein was
652 eluted with a KCl gradient. Eluted proteins were concentrated and further purified in gel
653 filtration buffer [25 mM tris-HCl pH 8.0, 150 mM KCl, 1 mM TCEP, 10% glycerol] using a
654 Superdex 75 10/300 GL size exclusion column (GE). Pure fractions were then concentrated,
655 aliquoted, flash-frozen in liquid nitrogen, and stored at −80 °C until further use.
656
657 *Peptide synthesis*
658 The PEAK1 peptide used for ITC was synthesized to >95% purity with acetylation at the N-
659 terminus and amidation at the C-terminus (Genscript). The peptide sequence was as follows:
660 KKWNTIPLRNKSLQRICAVDYDDSYD.
661
662 *Isothermal titration calorimetry*

663 ITC data were obtained using a Malvern Auto-iTC200 calorimeter (UMass Amherst). Peptide
664 was dissolved in gel filtration buffer with 6% v/v DMSO and concentration was determined
665 using ε280 = 8370 M-1cm-1. CAMK2 kinase domain was diluted in gel filtration buffer with
666 5.6% v/v DMSO and concentration was determined with ε280 = 43850 M-1cm-1. Titrations
667 were performed with the peptide as the titrant. Blank titrations were performed by injecting the
668 peptide into gel filtration buffer. All titrations were performed at 20 °C using the standard 19-
669 injection method where one injection of 0.4 µL is followed by 18 x 2 µL injections with 150 s
670 between injections. The stir speed was set to 750 rpm, and the reference power was set to 10.
671 Data were buffer-subtracted and analyzed using MicroCal ITC Origin add-on dissociation
672 model v1.00 using the one-site fitting model.
673
674 *Comparative modelling of PEAK1(291-320):CAMK2*
675 Several candidate structural models of PEAK1(291-320):CAMK2 were generated by
676 AlphaFold-Multimer[44, 45] (v3) using the ColabFold[46] (v1.5.1) community implementation.
677 Multiple sequence alignments and template searches were performed by MMseqs[44] and
678 HHsearch using default settings. Custom templates of CAMK2 in complex with known tight
679 binders were required to achieve models with acceptable metrics of pLTTD and pTM scores.
680 These interactions were manually curated from crystal structures determined by Özden et al[30]
681 (crystal symmetry mates were discarded). Six recycle rounds were conducted and final models
682 were ranked according to pTMscore. The best scoring models were relaxed with Amber[47] to
683 minimize steric clashes.
684
685 *Cross species multiple sequence alignment of PEAK1 N-terminus*
686 To generate a multiple sequence alignment, two rounds of PSI-BLAST[48] were performed
687 against the non-redundant clustered database[49] (to increase taxonomic depth) using human

688 PEAK1 as a query sequence. A cutoff of expectation value of $1x10^{-3}$ was used to select
689 sequences for subsequent rounds and alignment. Finally, the top 50 and top 250 sequences
690 (sorted by expectation value) were subjected to alignment in Clustal Omega[50, 51]. The full
691 sequence range for the top 250 sequences was subjected to a MEME[52] search to identify
692 consensus motifs.
693
694 *Proximity ligation assay (PLA)*
695 PLA was performed to detect protein-protein interactions in MDA-MB-231 cells using
696 Duolink™ In Situ Red Starter Kit (Sigma, cat. DUO92101). All the reagents, including probes,
697 detection reagents and wash buffers were provided in this kit. On day 1, $6x10^4$ cells were seeded
698 per well in a 48-well plate and incubated at 37 ºC overnight. On day 2, cells were gently washed
699 3 times with 1x phosphate-buffered saline [PBS; NaCl (136 mM), KCl (2.6 mM), Na2HPO4
700 (10 mM), KH2PO4 (1.76 mM)], and then fixed in 4% (v/v) paraformaldehyde (VWR, cat.
701 ALFA43368.9M) for 30 min on ice. Following that, cells were washed with 1xPBS again and
702 permeabilized with 0.2% Triton X-100 (Sigma, cat. T8787) for 3 min at room temperature.
703 After another 1xPBS washing step, cells were incubated with blocking solution for 30 min at
704 37 ºC, following which, cells were incubated with two primary antibodies from different
705 species against the targeted proteins overnight at 4 ºC. On day 3, cells were washed with 1x
706 Tris buffered saline (TBS) solution with the detergent Tween-20 [TBS-T; Tris base (50 mM),
707 NaCl (150 mM), pH 7.6, Tween-20 (0.01% v/v)], then PLA probes were added to the cells and
708 incubated for 60 min at 37 ºC. Following ligation and amplification steps, samples were
709 mounted with Mounting Medium with DAPI (Invitrogen, cat. P-36931). Cells were
710 photographed using a confocal microscope and dot numbers were analyzed using ImageJ
711 software (Version 1.52).
712

713 *Calcium Assay*

714 MDA-MB-231 EcoR cells expressing DsR empty vector, wildtype PEAK1 or PEAK1-CIM
715 mutants were generated by retroviral-mediated transduction as previously described[53]. Cells
716 were seeded into FluoroDish cell culture dishes (World Precision Instruments, cat. FD35-100)
717 and cultured overnight. The medium was then replaced with starvation medium (RPMI-1640
718 medium supplemented with 0.4% FBS, 10 µg/mL Actrapid penfill insulin, 20 mM HEPES)
719 supplemented with 5 µM Calcium indicator Fluo-4 AM (Invitrogen, cat. F14217). Cells were
720 then incubated for 60 min at 37°C. The dye-loading media was removed and replaced with
721 starvation medium without Fluo-4 AM. Images were acquired with a fluorescence microscope
722 (Leica DMi8) using the FITC filter set with excitation peaking at 495 nm and emission peaking
723 at 519 nm. The cellular fluorescence was quantitated using ImageJ software. A total of >200
724 cells were quantified per condition in each biological replicate. The background was subtracted
725 from the cell signal to plot fluorescence intensity.

726

727 *Proliferation assays*

728 These were performed using the CellTiter-Glo® 2.0 Cell Viability Assay (Promega – G9241)
729 as per the manufacturer's instructions. Briefly, MDA-MB-231 HM cells were harvested and
730 seeded into High Attachment (HA) (Falcon, FAL353072) and ultra-Low attachment (LA)
731 (Corning, CLS3474) plates at a density of 1000 cells/well. After 16-18h, Day 0 assays were
732 undertaken and the cells were treated either with vehicle control (DMSO) or RA306 at varying
733 concentrations. After 120 h, assays were performed on replicates of vehicle control and RA306-
734 treated cells.

735

736 *Transwell Migration/Invasion Assay*

737 Transwell migration and invasion assays were essentially as previously described[54]. Transwell

738 migration chambers with 8-µm pores were purchased from Corning (cat. CLS3464-48EA) and
739 MERCK Millipore (cat. MCEP24H48). Matrigel invasion chambers pre-coated with Matrigel
740 were purchased from Corning (cat. 354483). Prior to seeding, cells were treated with
741 mitomycin C at 10µg/ml for 1 h to prevent cell division.
742
743 *In vitro kinase assay*
744 HEK293T cells were transiently transfected with plasmids encoding wildtype PEAK1 or the
745 CAMK2-interaction motif mutants. Cell lysates were prepared using RIPA buffer[41]
746 supplemented with 12.5 mM β-glycerol phosphate. Cell lysates were then incubated with anti-
747 FLAG M2 affinity-agarose beads (Sigma, cat. A2220) at 4°C for 2 h with end-to-end rotation.
748 After the incubation, the beads were washed extensively with ice-cold RIPA buffer and kinase
749 reaction buffer [Tris (pH 7.5) 40 mM, $MgCl_2$ 10 mM, $CaCl_2$ 0.5 mM]. After the last wash,
750 beads were incubated in kinase reaction buffer supplemented with 100 ng recombinant
751 CAMK2D (Invitrogen, cat. PV3373), 100 µM recombinant calmodulin (Enzo, cat. BML-
752 SE325-0001) and 2 mM Adenosine 5'-triphosphate (ATP) disodium salt hydrate (Sigma-
753 Aldrich, cat. A1852-1VL) for 30 min at 37 ºC. Following incubation, the immune complexes
754 were eluted with SDS-PAGE loading buffer and subjected to Western blotting analysis.
755
756 *Animal Studies*
757 All procedures involving mice were conducted in accordance with National Health and
758 Medical Research Council (NHMRC) regulations on the use and care of experimental animals
759 and the study protocol approved by the Monash University Animal Ethics Committee.
760 Power calculations performed indicated group sizes of n = 8 per treatment group were required
761 to detect a significant difference in tumor growth inhibition of 50% between treated and control
762 (significance level: 0.05; power: 90%). All *in vivo* experiments were performed with 6-week-

763 old female BALB/c athymic nude mice obtained from the Animal Resources Centre (Canning
764 Vale, Australia) and housed in sterile conditions at Monash Animal Research Platform.
765 Throughout the study, each cage was randomly assigned to the experimental groups without
766 considering any other variable. Mice were randomly divided into four equal groups, cas9-
767 control cells with captisol (control), cas9-control cells with RA306, cas9-sgPEAK1 cells with
768 captisol and cas9-sgPEAK1 cells with RA306.
769
770 *Xenograft model*
771 Mice (n=40) were injected with 2×10^5 MDA-MB-231_HM Cas9 control or sgPEAK1 stable
772 knockdown cells suspended in 20µl PBS into the fourth mammary fat pad. One day post-
773 injection, RA306 (30mg/kg) or captisol-only control was administered via daily oral gavage
774 until the end of the experiment. To measure tumour burden, mice were injected with luciferin
775 (150 mg/kg) by an intraperitoneal route. Tumour burden was measured weekly using the AMI-
776 HTX imaging system (Spectral Instruments Imaging). Results are presented as mean +/- SEM
777 of total BLI signal (photons/s).
778
779 *Tumour metastasis model*
780 Mice (n=40) were injected with 2×10^5 MDA-MB-231_HM Cas9 control or sgPEAK1 stable
781 knockdown cells suspended in 20µl PBS into the fourth mammary fat pad. One day post-
782 injection, RA306 (30mg/kg) or captisol-only control was administered via daily oral gavage
783 until the end of the experiment. When the primary tumours from each group reached ~ 100
784 mm^3 in size, they were resected. Tumour metastasis to secondary sites was then measured
785 weekly using the AMI-HTX imaging system (Spectral Instruments Imaging). Organs were
786 dissected immediately following the final BLI image and re-imaged in the AMI-HTX ex vivo
787 to allow for direct measurement of organ-specific tumour burden via BLI. Results are presented

788 as mean tumour luciferase intensities +/- SEM of total BLI signal (photons/s).

789

790 *Tumour tissue homogenization*

791 Following dissection at the experimental endpoint, tumour tissues were transferred
792 immediately to dry ice. Tumour tissues were cut into small pieces and added to a 1.5ml tube
793 containing RIPA buffer and Zirconia tissue disruption beads (Research Products International,
794 cat. 9835) then homogenized for 10s at low speed and 30s at high speed at room temperature.
795 To prepare samples for Western blotting, homogenized samples were centrifuged for 20 min
796 at 20,000g at 4ºC. The supernatant was then collected and the protein concentration determined
797 using either Bradford Ultra Protein Assay Reagent (Expedeon, cat. EP-BFU05L) or Pierce TM
798 BCA Protein Assay Reagents (Thermo Scientific, cat. 23225). The protein concentration of
799 each sample was subsequently adjusted using RIPA buffer, and SDS-PAGE loading buffer was
800 added prior to Western blotting analysis.

801

802 *Association of PEAK1 and CAMK2D/G with overall survival and distant metastasis-free*
803 *survival*

804 For overall survival analysis, mRNA expression, mutation profile and associated overall
805 survival data from 2509 breast cancer patients as part of the METABRIC trial [55] were
806 downloaded from the cBioPortal for Cancer Genomics portal (https://www.cbioportal.org/).
807 Breast cancer patients were divided and classified into three main groups each having either
808 low, or medium, or high expression of *CAMK2D, CAMK2G* or *PEAK1*, individually. Main
809 groups were then further categorised into four sub-groups exhibiting different combined
810 expression patterns: *i) CAMK2D* and *PEAK1* both high, *ii) CAMK2D* and *PEAK1* both low,
811 *iii) CAMK2G* and *PEAK1* both high, *iv) CAMK2G* and *PEAK1* both low, *v) CAMK2D* low and
812 *PEAK1* high, *vi) CAMK2D* high and *PEAK1* low. Survival analyses comparing overall survival

813 between these sub-groups were subsequently performed using a Log-rank test (with $p < 0.05$
814 considered significant). The Log-rank test statistics and survival curves were generated using
815 Kaplan-Meier estimate and implemented using the Logrank package [55] in MATLAB 2023a.
816 To determine association with distant metastasis-free survival (DMFS), mRNA expression and
817 DMFS data were obtained for the following cohorts in the Gene Expression Omnibus (GEO)
818 database: Princess Margaret Cancer Centre (database accesssions GSE6532 and GSE9195),
819 Veridex LLC (GSE12093) and Bayer Technology Services GmbH (GSE11121). CAMK2D
820 data were unavailable in most datasets; therefore, this analysis focused on PEAK1 and
821 CAMK2G. To create a more robust and larger meta-dataset we applied z-score standardization
822 to the gene expression data of individual cohorts and then combined all cohort data to generate
823 a 527 patient meta-cohort. Subsequently, breast cancer patients were divided into low or high
824 expression groups for PEAK1 and CAMK2G, individually, based on the 33% percentile of
825 gene expression (bottom 33% vs top 67%). Finally, patient groups were categorized into two
826 subgroups based on combined expression patterns: *i)* PEAK1 and CAMK2G both low, and *ii)*
827 PEAK1 and CAMK2G both high. The DMFS was compared between these two subgroups
828 using a log-rank test ($p < 0.05$ considered significant). Log-rank test statistics and survival
829 curves were generated using the *survival* (version 3.5.8) and *survminer* (version 0.4.9)
830 packages in R.
831
832 *Statistical analyses*
833 Experimental data were subject to appropriate statistical analyses as detailed in the
834 corresponding figure legends.
835
836 *Data availability*

837 The mass spectrometry proteomics data for the spectral library and DIA analysis have been
838 deposited to the ProteomeXchange Consortium via the PRIDE[56] partner repository with the
839 dataset identifier PXD044872.
840 Reviewer account details:
841 Username: reviewer_pxd044872@ebi.ac.uk
842 Password: LHFHdDGH
843 The remaining data are available within the Article, Supplementary Information or Source Data
844 file.
845
846 **References**
847

848 1. Reiterer V, Eyers PA, Farhan H. Day of the dead: pseudokinases and
849 pseudophosphatases in physiology and disease. *Trends Cell Biol* **24**, 489-505 (2014).
850
851 2. Zeqiraj E, van Aalten DM. Pseudokinases-remnants of evolution or key allosteric
852 regulators? *Current opinion in structural biology* **20**, 772-781 (2010).
853
854 3. Kung JE, Jura N. Prospects for pharmacological targeting of pseudokinases. *Nat Rev*
855 *Drug Discov* **18**, 501-526 (2019).
856
857 4. Hou J*, et al.* Distinct PEAK3 interactors and outputs expand the signaling potential of
858 the PEAK pseudokinase family. *Sci Signal* **15**, eabj3554 (2022).
859
860 5. Patel O, Roy MJ, Murphy JM, Lucet IS. The PEAK family of pseudokinases, their
861 role in cell signalling and cancer. *FEBS J* **287**, 4183-4197 (2020).
862
863 6. Croucher DR*, et al.* Involvement of Lyn and the atypical kinase SgK269/PEAK1 in a
864 basal breast cancer signaling pathway. *Cancer Res* **73**, 1969-1980 (2013).
865
866 7. Agajanian M*, et al.* PEAK1 Acts as a Molecular Switch to Regulate Context-
867 Dependent TGFbeta Responses in Breast Cancer. *PLoS One* **10**, e0135748 (2015).
868
869 8. Abu-Thuraia A*, et al.* AXL confers cell migration and invasion by hijacking a
870 PEAK1-regulated focal adhesion protein network. *Nature communications* **11**, 1-20
871 (2020).
872
873 9. Ding C*, et al.* Overexpression of PEAK1 contributes to epithelial-mesenchymal
874 transition and tumor metastasis in lung cancer through modulating ERK1/2 and JAK2
875 signaling. *Cell Death Dis* **9**, 802 (2018).
876

877 10. Kelber JA, *et al.* KRas induces a Src/PEAK1/ErbB2 kinase amplification loop that
878 drives metastatic growth and therapy resistance in pancreatic cancer. *Cancer Res* **72**,
879 2554-2564 (2012).
880
881 11. Leroy C, *et al.* Quantitative phosphoproteomics reveals a cluster of tyrosine kinases
882 that mediates SRC invasive activity in advanced colon carcinoma cells. *Cancer Res*
883 **69**, 2279-2286 (2009).
884
885 12. Ounoughene Y, *et al.* SHED-Dependent Oncogenic Signaling of the PEAK3 Pseudo-
886 Kinase. *Cancers (Basel)* **13**, (2021).
887
888 13. Senda Y, Murata-Kamiya N, Hatakeyama M. C-terminal Src kinase-mediated EPIYA
889 phosphorylation of Pragmin creates a feed-forward C-terminal Src kinase activation
890 loop that promotes cell motility. *Cancer Sci* **107**, 972-980 (2016).
891
892 14. Tactacan CM, *et al.* The pseudokinase SgK223 promotes invasion of pancreatic
893 ductal epithelial cells through JAK1/Stat3 signaling. *Mol Cancer* **14**, 139 (2015).
894
895 15. Lecointre C, *et al.* Oncogenic Signalling of PEAK2 Pseudokinase in Colon Cancer.
896 *Cancers (Basel)* **14**, (2022).
897
898 16. Liu L, *et al.* Homo- and Heterotypic Association Regulates Signaling by the
899 SgK269/PEAK1 and SgK223 Pseudokinases. *J Biol Chem* **291**, 21571-21583 (2016).
900
901 17. Ha BH, Boggon TJ. The crystal structure of pseudokinase PEAK1 (Sugen kinase 269)
902 reveals an unusual catalytic cleft and a novel mode of kinase fold dimerization. *J Biol*
903 *Chem* **293**, 1642-1650 (2018).
904
905 18. Patel O, *et al.* Structure of SgK223 pseudokinase reveals novel mechanisms of
906 homotypic and heterotypic association. *Nat Commun* **8**, 1157 (2017).
907
908 19. Zheng Y, *et al.* Temporal regulation of EGF signalling networks by the scaffold
909 protein Shc1. *Nature* **499**, 166-171 (2013).
910
911 20. Brzozowski JS, Skelding KA. The Multi-Functional Calcium/Calmodulin Stimulated
912 Protein Kinase (CaMK) Family: Emerging Targets for Anti-Cancer Therapeutic
913 Intervention. *Pharmaceuticals (Basel)* **12**, (2019).
914
915 21. Chi M, *et al.* Phosphorylation of calcium/calmodulin-stimulated protein kinase II at
916 T286 enhances invasion and migration of human breast cancer cells. *Sci Rep* **6**, 33132
917 (2016).
918
919 22. Croucher DR, *et al.* Bimolecular complementation affinity purification (BiCAP)
920 reveals dimer-specific protein interactions for ERBB2 dimers. *Sci Signal* **9**, ra69
921 (2016).
922
923 23. Roy MJ, *et al.* Structural mapping of PEAK pseudokinase interactions identifies 14-3-
924 3 as a molecular switch for PEAK3 signaling. *Nat Commun* **14**, 3542 (2023).
925

24. Bhattacharyya M, Karandur D, Kuriyan J. Structural Insights into the Regulation of Ca(2+)/Calmodulin-Dependent Protein Kinase II (CaMKII). *Cold Spring Harb Perspect Biol* **12**, (2020).

25. Tsien RY. A non-disruptive technique for loading calcium buffers and indicators into cells. *Nature* **290**, 527-528 (1981).

26. Mandal S, Bandyopadhyay S, Tyagi K, Roy A. Recent advances in understanding the molecular role of phosphoinositide-specific phospholipase C gamma 1 as an emerging onco-driver and novel therapeutic target in human carcinogenesis. *Biochim Biophys Acta Rev Cancer* **1876**, 188619 (2021).

27. Hochgrafe F*, et al.* Tyrosine phosphorylation profiling reveals the signaling network characteristics of Basal breast cancer cells. *Cancer Res* **70**, 9391-9401 (2010).

28. Jones NP, Peak J, Brader S, Eccles SA, Katan M. PLCgamma1 is essential for early events in integrin signalling required for cell motility. *J Cell Sci* **118**, 2695-2706 (2005).

29. Temps C*, et al.* A Conformation Selective Mode of Inhibiting SRC Improves Drug Efficacy and Tolerability. *Cancer Res* **81**, 5438-5450 (2021).

30. Ozden C*, et al.* CaMKII binds both substrates and activators at the active site. *Cell Rep* **40**, 111064 (2022).

31. Saneyoshi T*, et al.* Reciprocal Activation within a Kinase-Effector Complex Underlying Persistence of Structural LTP. *Neuron* **102**, 1199-1210 e1196 (2019).

32. Beauverger P*, et al.* Reversion of cardiac dysfunction by a novel orally available calcium/calmodulin-dependent protein kinase II inhibitor, RA306, in a genetic model of dilated cardiomyopathy. *Cardiovasc Res* **116**, 329-338 (2020).

33. Yang X*, et al.* The pseudokinase NRBP1 activates Rac1/Cdc42 via P-Rex1 to drive oncogenic signalling in triple-negative breast cancer. *Oncogene* **42**, 833-847 (2023).

34. Lecointre C*, et al.* Dimerization of the Pragmin Pseudo-Kinase Regulates Protein Tyrosine Phosphorylation. *Structure* **26**, 545-554 e544 (2018).

35. Sausgruber N*, et al.* Tyrosine phosphatase SHP2 increases cell motility in triple-negative breast cancer through the activation of SRC-family kinases. *Oncogene* **34**, 2272-2278 (2015).

36. Bristow JM, Reno TA, Jo M, Gonias SL, Klemke RL. Dynamic phosphorylation of tyrosine 665 in pseudopodium-enriched atypical kinase 1 (PEAK1) is essential for the regulation of cell migration and focal adhesion turnover. *J Biol Chem* **288**, 123-131 (2013).

37. Yu G*, et al.* Organelle-Derived Acetyl-CoA Promotes Prostate Cancer Cell Survival, Migration, and Metastasis via Activation of Calmodulin Kinase II. *Cancer Res* **78**, 2490-2502 (2018).

38. Ren D, *et al.* Targeting Brain-Adaptive Cancer Stem Cells Prohibits Brain Metastatic Colonization of Triple-Negative Breast Cancer. *Cancer Res* **78**, 2052-2064 (2018).

39. Easley CA, Brown CM, Horwitz AF, Tombes RM. CaMK-II promotes focal adhesion turnover and cell motility by inducing tyrosine dephosphorylation of FAK and paxillin. *Cell Motil Cytoskeleton* **65**, 662-674 (2008).

40. Pellicena P, Schulman H. CaMKII inhibitors: from research tools to therapeutic agents. *Front Pharmacol* **5**, 21 (2014).

41. Brummer T, *et al.* Increased proliferation and altered growth factor dependence of human mammary epithelial cells overexpressing the Gab2 docking protein. *Journal of Biological Chemistry* **281**, 626-637 (2006).

42. Cox J, Mann M. MaxQuant enables high peptide identification rates, individualized p.p.b.-range mass accuracies and proteome-wide protein quantification. *Nat Biotechnol* **26**, 1367-1372 (2008).

43. Tyanova S, *et al.* The Perseus computational platform for comprehensive analysis of (prote)omics data. *Nat Methods* **13**, 731-740 (2016).

44. Evans R, *et al.* Protein complex prediction with AlphaFold-Multimer. *bioRxiv*, 2021.2010.2004.463034 (2022).

45. Jumper J, *et al.* Highly accurate protein structure prediction with AlphaFold. *Nature* **596**, 583-589 (2021).

46. Mirdita M, Schutze K, Moriwaki Y, Heo L, Ovchinnikov S, Steinegger M. ColabFold: making protein folding accessible to all. *Nat Methods* **19**, 679-682 (2022).

47. Hornak V, Abel R, Okur A, Strockbine B, Roitberg A, Simmerling C. Comparison of multiple Amber force fields and development of improved protein backbone parameters. *Proteins* **65**, 712-725 (2006).

48. Altschul SF, *et al.* Gapped BLAST and PSI-BLAST: a new generation of protein database search programs. *Nucleic Acids Res* **25**, 3389-3402 (1997).

49. Steinegger M, Soding J. MMseqs2 enables sensitive protein sequence searching for the analysis of massive data sets. *Nat Biotechnol* **35**, 1026-1028 (2017).

50. McWilliam H, *et al.* Analysis Tool Web Services from the EMBL-EBI. *Nucleic Acids Res* **41**, W597-600 (2013).

51. Sievers F, *et al.* Fast, scalable generation of high-quality protein multiple sequence alignments using Clustal Omega. *Mol Syst Biol* **7**, 539 (2011).

52. Bailey TL, Elkan C. Fitting a mixture model by expectation maximization to discover motifs in biopolymers. *Proc Int Conf Intell Syst Mol Biol* **2**, 28-36 (1994).

1026 53. Croucher DR, Rickwood D, Tactacan CM, Musgrove EA, Daly RJ. Cortactin
1027 modulates RhoA activation and expression of Cip/Kip cyclin-dependent kinase
1028 inhibitors to promote cell cycle progression in 11q13-amplified head and neck
1029 squamous cell carcinoma cells. *Mol Cell Biol* **30**, 5057-5070 (2010).
1030
1031 54. Bennett HL, Brummer T, Jeanes A, Yap AS, Daly RJ. Gab2 and Src co-operate in
1032 human mammary epithelial cells to promote growth factor independence and
1033 disruption of acinar morphogenesis. *Oncogene* **27**, 2693-2704 (2008).
1034
1035 55. Pereira B*, et al.* The somatic mutation profiles of 2,433 breast cancers refines their
1036 genomic and transcriptomic landscapes. *Nat Commun* **7**, 11479 (2016).
1037
1038 56. Perez-Riverol Y*, et al.* The PRIDE database resources in 2022: a hub for mass
1039 spectrometry-based proteomics evidences. *Nucleic Acids Res* **50**, D543-D552 (2022).
1040
1041

1042 **Acknowledgements**

1043 The authors acknowledge the Monash Proteomics and Metabolomics Facility, Monash
1044 University, for the provision of MS instrumentation, training and technical support, and
1045 Monash Micro Imaging for assistance with the calcium imaging experiments. The work was
1046 supported by research grants to RJD from the National Health and Medical Research Council
1047 of Australia (Ideas Grant 2003599) and Australian Research Council (ARC) (DP220103638
1048 and DP190103672) and to MMS (NIH R35GM145376). DRC acknowledges fellowship
1049 support from the National Breast Cancer Foundation (NBCF Fellowship IIRS-20-032), AME
1050 is a Victorian Department of Health and Human Services Victorian Cancer Agency Mid-Career
1051 Fellow (MCRF21036) and CB is an ARC DECRA Fellow (DE240100992). VCBN is a
1052 member of the Molecular and Cellular Biology Graduate Program, University of
1053 Massachusetts, Amherst, MA 01003, USA and is supported by a fellowship from the
1054 University of Massachusetts as part of the Chemistry-Biology Interface Training Program
1055 (National Research Service Award T32 GM139789).

1056

1057 **Author Contributions**

1058 Conceptualization, RJD; Methodology, XY, XM, DRC, CB, SB, SS, LKN, ACC, MMS, AME,
1059 RJD; Investigation, XY, XM, DRC, EVN, KCC, CH, SLL, TZ, CB, VCBN, SB, SS, TCCLKS;
1060 Writing – Original Draft, XY, XM, RJD; Writing – Review and Editing, TRC, MMS, AME,
1061 RJD; Visualization, XY, TRC, RJD; Funding acquisition, DRC, MMS, CB, AME, RJD;
1062 Supervision, XM, RJD; Project administration, RJD.
1063
1064 **Declaration of interests**
1065 The authors declare that they have no competing interests.
1066
1067 **Figure Legends**
1068
1069 **Figure 1. Identification of specific CAMK2 isoforms as PEAK1/2 interactors via BiCAP-**
1070 **MS/MS. A-C. Results of BiCAP-MS/MS screen.** Volcano plots indicate enriched interactors
1071 for the PEAK1 homotypic complex (A), PEAK2 homotypic complex (B) and PEAK1/PEAK2
1072 heterotypic complex (C). The known PEAK1 interactor Grb2 and targets of particular interest,
1073 including specific CAMK2 family members, are highlighted in blue. Dotted lines indicate fold
1074 change and p value cut-offs. **D. Western blotting validation of PEAK1 and PEAK2**
1075 **knockdown.** PEAK1 and PEAK2 were knocked down using siRNA pools, with successful
1076 knockdown confirmed by Western blotting. **E-F. Validation of PEAK1/2 association with**
1077 **CAMK2D and CAMK2G by proximity ligation assays.** Left panels, representative
1078 proximity ligation assay (PLA) images from MDA-MB-231 cells for interaction of PEAK1 (E)
1079 or PEAK2 (F) with CAMK2D and CAMK2G. Cells were transfected with either si-PEAK1
1080 (E), si-PEAK2 (F) or si-Control. Right panels, quantification of protein interactions in each
1081 cell. The data are expressed as dot number divided by cell number. In each condition, more

1082 than 50 cells have been counted. Error bars represent the standard error of the mean from n=3
1083 independent experiments. * = $p < 0.05$, ** = $p < 0.01$ by student's t-test.
1084
1085 **Figure 2. PEAK1-mediated regulation of CAMK2 activity in triple negative breast cancer**
1086 **cells. A-D. Manipulation of PEAK1 expression modulates CAMK2 activity.** PEAK1 was
1087 knocked down using a siRNA (A-B) or overexpressed via transient transfection (C-D) in MDA-
1088 MB-231 cells and autonomous activation of CAMK2 determined by Western blotting as
1089 indicated. Blotting for 14-3-3 served as a loading control. Histograms indicate CAMK2 T287
1090 phosphorylation normalized for total CAMK2 expression, with 'au' indicating arbitrary units.
1091 **E-F. PEAK1-promoted CAMK2 activation is calcium-dependent.** MDA-MB-231 cells
1092 were transfected with a PEAK1 construct in the presence or absence of 10 μM BAPTA-AM.
1093 Cell lysates were Western blotted as indicated (E) and CAMK2 activation quantified as above
1094 for CAMK2D/G combined (F), with data expressed relative to the DsR (vector)/DMSO control
1095 which was arbitrarily set at 1. **G-H. Overexpression of PEAK1 increases intracellular Ca^{2+}.**
1096 MDA-MB-231_EcoR cells stably overexpressing PEAK1 were loaded with calcium-sensitive
1097 dye Fluo-4 AM and then imaged with a fluorescence microscope. Representative images from
1098 3 independent experiments are shown (G) as well as quantification of Fluo-4 images (H),
1099 presented as mean Fluo-4 fluorescence ± SEM. These are representative data from one
1100 biological replicate from a total of three. **I-J. PEAK1 regulates tyrosine phosphorylation of**
1101 **PLCγ1.** MDA-MB-231 cells were transfected with PEAK1 siRNA (I) or a PEAK1 expression
1102 vector (J) and then cell lysates were Western blotted as indicated. The histograms indicate
1103 Y783-phosphorylated PLCγ1 normalized for total PLCγ1 expression. For all panels, error bars
1104 represent the standard error of the mean from n=3 independent experiments. NS indicates $p >$
1105 0.05, * = $p < 0.05$, ** = $p<0.01$, *** = $p<0.001$, ****, $p < 0.0001$, by ratio paired t-test (B, D,
1106 I, J), two-way ANOVA with Tukey's multiple comparisons test (F), or unpaired t-test (H).

1107

1108 **Figure 3. Mapping the CAMK2 binding region on PEAK1. A. Schematic structure of**
1109 **PEAK1 and various truncation mutants**. WT, wildtype. **B. Association of CAMK2D with**
1110 **specific PEAK1 deletion mutants.** The indicated Flag-tagged PEAK1 deletion mutants were
1111 expressed in HEK293T cells. Total cell lysates (TCL) and Flag IPs were subjected to Western
1112 blotting as indicated. **C. Schematic representation of various PEAK1 N-terminal deletion**
1113 **mutants.** Deleted regions of PEAK1 are indicated by red crosses. **D-E. Fine structure**
1114 **mapping of N-terminal regions required for the association of PEAK1 with CAMK2D**
1115 **(D) or CAMK2G (E).** Analysis was undertaken as in (B). The asterisk in 3D highlights
1116 degradation products present for the Δ261-300 and Δ261-324 mutants. **F-G. PEAK1 binding**
1117 **to CAMK2 is required for CAMK2 activation.** MDA-MB-231 cells were transfected with
1118 WT PEAK1 or the Δ301-324 PEAK1 construct. Cell lysates were Western blotted as indicated
1119 (F), with the dotted line in F indicating where the image was cropped to remove an irrelevant
1120 lane. Raw data for the full image accompanies the manuscript. Relative CAMK2 activation,
1121 as determined by T287 phosphorylation, was then quantified (G). Data are expressed relative
1122 to vector control which was arbitrarily set at 1. All data in B, D and E are representative of at
1123 least 2 independent experiments. In G, error bars represent the standard error of the mean from
1124 n=3 independent experiments. NS indicates $p > 0.05$, * = $p < 0.05$ by one-way ANOVA with
1125 Tukey's multiple comparisons test.

1126

1127 **Figure 4. Characterization of a conserved CAMK2 interaction motif (CIM) on PEAK1.**
1128 **A. Sequence alignment of the PEAK1 CIM with other CAMK2 binding partners**. The
1129 critical residues for CAMK2 interaction (R297, L301 and R303 in PEAK1) are highlighted in
1130 yellow. The canonical motif numbering (A306 being 0) is shown above the alignment. **B.**
1131 **Representative ITC measurement of CAMK2 kinase domain binding to PEAK1 CIM**

1132 **peptide.** The mean Kd value from n=3 independent experiments is indicated. **C. Comparative**
1133 **modelling of the PEAK1/CAMK2 interaction by AlphaFold.** Surface representation of
1134 CAMK2 with PEAK1 amino acids 291-320 shown as ribbon (grey). The orientation is as in
1135 Supp Figure 6. CAMK2 is coloured by electrostatic charge. The PEAK1 binding site on
1136 CAMK2 is noticeably negative, with key arginine residues of PEAK1 mediating interactions
1137 with CAMK2. The N- and C-termini are labelled as N and C, respectively. **D. Surface**
1138 **representation of modelled PEAK1/CAMK2 interaction.** CAMK2 is grey and PEAK1
1139 amino acids 291-320 are purple. **E-F. Focused view of key predicted molecular interactions.**
1140 Boxed regions from (D) illustrating predicted formation of salt bridges and electrostatic
1141 interactions (dotted lines) by specific PEAK1 residues across the surface of CAMK2. The
1142 canonical numbering of the PEAK1 motif is shown in white boxes.
1143
1144 **Figure 5. The role of the PEAK1 CIM in CAMK2 activation. A-B. Effect of CIM mutation**
1145 **on intracellular Ca^{2+} levels.** Constructs expressing WT PEAK1 or the indicated mutants were
1146 stably expressed in MDA-MB-231_EcoR cells via retroviral transduction. PEAK1 expression
1147 levels were determined by Western blot (A) and Ca^{2+} levels (B) assayed as in Figure 2G-H.
1148 Data in B represent mean Fluo-4 fluorescence ± SEM from one representative biological
1149 replicate from a total of two independent experiments. Statistical analysis utilized one way
1150 ANOVA with Dunnett's multiple comparisons test with **** indicating $p < 0.0001$. **C-D.**
1151 **Effect of CIM mutation on tyrosine phosphorylation of PLCγ1**. The indicated plasmids
1152 were transiently transfected into HEK293 cells and cell lysates Western blotted as indicated
1153 (C). PLCγ1 tyrosine phosphorylation was normalized for total expression (D). Data in D are
1154 expressed relative to the vector control which was arbitrarily set at 1 and represent the mean ±
1155 SEM of 3 independent biological replicates, * indicates $p<0.05$ by unpaired t-test. **E-G. Effect**
1156 **of CIM mutation on CAMK2 activation.** Plasmids encoding WT PEAK1 and the indicated

1157 mutants were transfected into MDA-MB-231 cells. Total cell lysates were Western blotted as
1158 indicated (E) and then relative CAMK2 activation was quantified (F-G). Data are expressed
1159 relative to the vector (DsR) control which was arbitrarily set at 1. NS indicates $p > 0.05$, ** =
1160 $p < 0.01$ and **** = $p < 0.0001$ by one-way ANOVA with Dunnett's multiple comparisons
1161 test.
1162
1163 **Figure 6. CAMK2 phosphorylates PEAK1 to regulate the PEAK1 interactome. A-B.**
1164 **RA306 inhibits PEAK1 serine/threonine phosphorylation.** MDA-MB-231_EcoR cells
1165 stably expressing Flag-tagged PEAK1 were treated with RA306 (1 μM) for 24 h and cell lysates
1166 were directly Western blotted or subject to immunoprecipitation with Flag antibody prior to
1167 blotting as indicated (A). Relative serine/threonine phosphorylation of PEAK1, normalized for
1168 total PEAK1, is shown in the histogram (B). **C. CAMK2 phosphorylates PEAK1 *in vitro*.**
1169 Flag-tagged versions of WT and mutant PEAK1 proteins were expressed in HEK293T cells.
1170 PEAK1 proteins were immunoprecipitated using anti-Flag antibody and following washing,
1171 immediately treated with SDS-PAGE sample buffer (SB) (no incubation) or incubated in
1172 kinase reaction buffer supplemented as indicated at 37°C for 30 min. Reactions were terminated
1173 with SB. Samples were then Western blotted as indicated. The asterisk indicates a background
1174 band present in all CAMK2D-incubated samples including the vector control while the
1175 arrowhead highlights phosphorylated PEAK1. **D. Impact of CIM mutations on heterotypic**
1176 **association with PEAK2.** Flag-tagged WT PEAK1 or PEAK1 mutants were expressed in
1177 MDA-MB-231 cells and association with endogenous PEAK2 assayed by IP/Western. For
1178 panel B, * = $p<0.05$ by ratio paired t-test.
1179
1180 **Figure 7. Role of CAMK2 in PEAK1-regulated biological endpoints in TNBC models. A.**
1181 **PEAK1 overexpression in combination with CAMK2D and CAMK2G knockdown in**

1182 **MDA-MB-231 cells.** Cells were transfected with a PEAK1 plasmid in the presence or absence
1183 of siRNA-mediated CAMK2D or CAMK2G knockdown. Cell lysates were Western blotted as
1184 indicated. **B. Role of CAMK2D/G in PEAK1-promoted MDA-MB-231 cell migration.**
1185 Cells validated in (A) were subjected to a transwell migration assay. **C-D**, **Role of CAMK2**
1186 **activation.** MDA-MB-231 cells were transfected with a PEAK1 plasmid and subject to
1187 transwell migration assays in the presence or absence of RA306 (C)**.** Plasmids expressing WT
1188 PEAK1 and the Δ301-324 mutant that cannot activate CAMK2 were transiently transfected
1189 into MDA-MB-231 cells, and cells were subjected to a transwell migration assay (D). **E. Role**
1190 **of PEAK1/CAMK2 signalling in TNBC xenograft growth.** Control MDA-MB-231_HM
1191 cells (Cas9-control) or PEAK1 KO cells (Cas9-sgPEAK1) in combination with RA306 or
1192 vehicle control (captisol) were injected into the mammary fat pad. Left panel, representative
1193 whole body bioluminescent imaging (BLI) images from each group at different time points as
1194 indicated. Right panel, quantification of xenograft growth. Each treatment group exhibited ≥ 9
1195 mice. **F. Role of PEAK1/CAMK2 signalling in TNBC metastasis.** Control MDA-MB-
1196 231_HM cells (Cas9-control) or PEAK1 KO cells (Cas9-sgPEAK1) in combination with
1197 RA306 or vehicle control (captisol) were injected into the mammary fat pad. At Day 19 post-
1198 injection when the primary tumour from each group reached ~ 100 mm^3, they were resected,
1199 and tumour growth at secondary sites was measured. Left panel, representative whole body and
1200 *ex vivo* lung BLI images from each group at Day 72 post injection. Right panel, luciferase
1201 intensities of tumour metastasis to lung were generated from each group. Error bars represents
1202 the standard error of the mean from n=3 independent experiments (B-D) or from the individuals
1203 of each group (E & F). NS indicates $p > 0.05$, * = $p < 0.05$, ** = $p < 0.01$, *** = $p < 0.001$,
1204 **** = $p < 0.0001$ by two-way ANOVA with Tukey's multiple comparisons test (B, C, E),
1205 one-way ANOVA with Tukey's multiple comparisons test (D), or one-way ANOVA with
1206 Dunnett's multiple comparisons test (F).

1207

1208 **Figure 8. Schematic representation of feed-forward regulation of CAMK2 by PEAK1.**
1209 PEAK1 enhances intracellular Ca^{2+} by promoting SFK-mediated tyrosine phosphorylation of
1210 PLCγ1. This leads to classical activation of CAMK2 by Ca^{2+}/CaM and the αD helix rotates
1211 out. The PEAK1 CIM then binds to the CAMK2 substrate binding site and competes with the
1212 regulatory segment, effectively 'locking' CAMK2 in an active conformation. Sustained
1213 phosphorylation of PEAK1 and CAMK2 itself (on T287) then occurs as the PEAK1 CIM
1214 undergoes cycles of dissociation and re-association. However, other mechanisms may
1215 contribute to the observed effects on CAMK2 activation, as indicated on the figure. CIM-
1216 mediated recruitment of PEAK1 to the CAMK2 holoenzyme promotes serine/threonine
1217 phosphorylation of PEAK1 which in turn positively regulates heterotypic association with
1218 PEAK2.

1219

1220 **Supplementary Information Titles and Legends**

1221

1222 Supp.Table 1. BiCAP-MS/MS data for PEAK dimer-specific interactomes.

1223 Supp.Table 2. Pathway enrichment analysis for dimer-specific interactomes.

1224

1225 Supp. Figure 1. Characterization of PEAK complex interactomes via BiCAP-MS/MS.

1226 Supp. Figure 2. Manipulation of PEAK1 expression modulates CAMK2 activity in MDA-MB-
1227 468 cells.

1228 Supp. Figure 3. Effect of SFK inhibitor eCF506 on PLCγ1 Y783 phosphorylation.

1229 Supp. Figure 4. Determination of the structural requirements for CAMK2 interaction with
1230 PEAK2.

1231 Supp. Figure 5. Sequence alignment of the PEAK1 CIM motif across diverse species.

1232 Supp. Figure 6. Comparative modelling analysis by AlphaFold (to accompany Figure 4C-F).

1233 Supp. Figure 7. Role of CAMK2 in regulating PEAK1 phosphorylation and the PEAK1
1234 interactome.

1235 Supp. Figure 8. Association of PEAK1 and CAMK2 expression with breast cancer patient
1236 survival.

1237 Supp. Figure 9. Effect of the CAMK2 inhibitor RA306 on cell proliferation and apoptosis.

1238 Supp. Figure 10. Role of CAMK2 in PEAK1-regulated biological endpoints in TNBC models.

1239 Supp. Figure 11. Genetic or pharmacological targeting of the PEAK1/CAMK2 axis reduces
1240 TNBC development *in vivo*.

1241

1242

Figure 1.

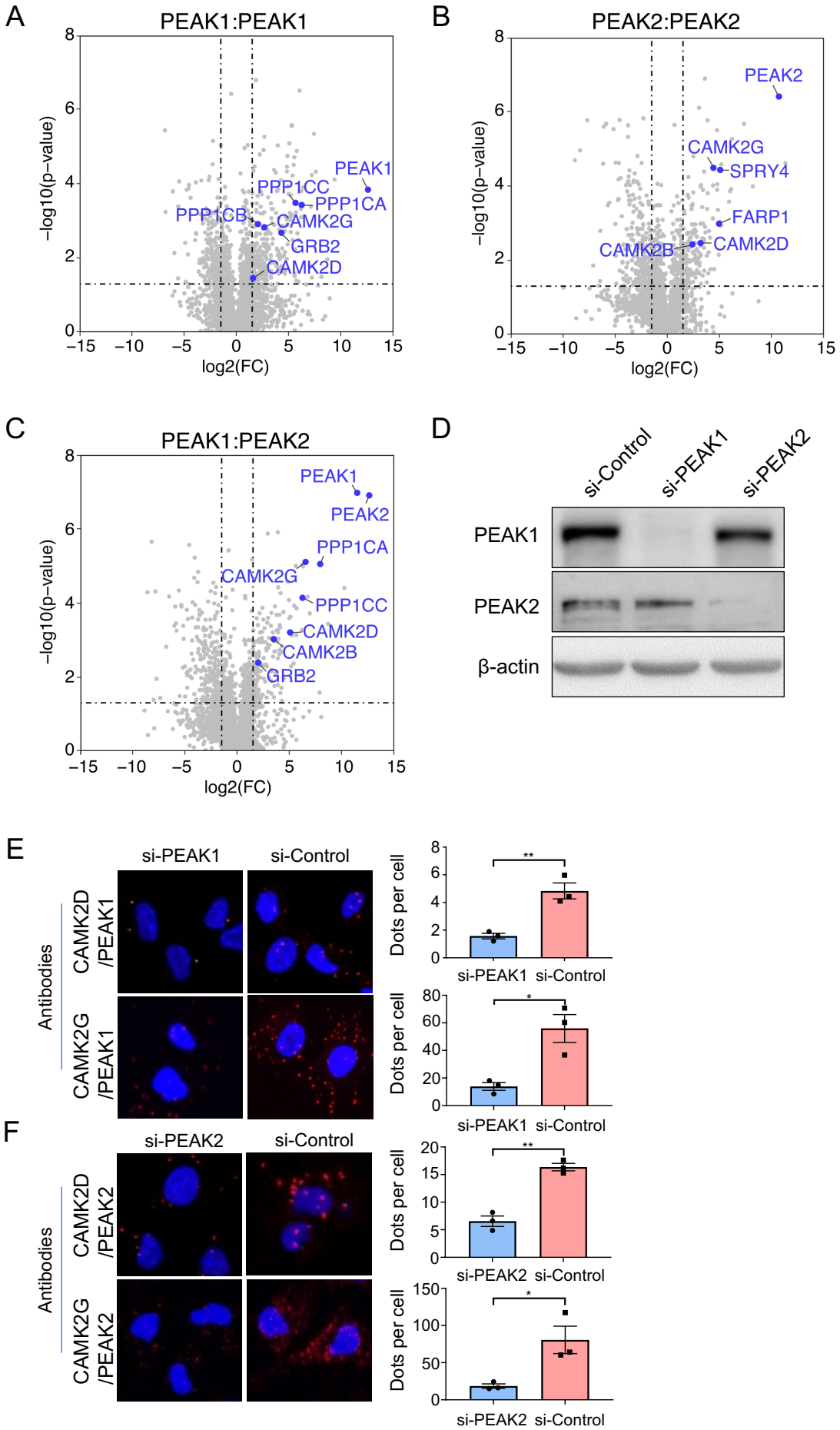
A
PEAK1:PEAK1
−log10(p−value)
log2(FC)
PEAK1
PPP1CC
PPP1CA
PPP1CB
CAMK2G
GRB2
CAMK2D
B
PEAK2:PEAK2
PEAK2
CAMK2G
SPRY4
FARP1
CAMK2B
CAMK2D
C
PEAK1:PEAK2
PEAK1
PEAK2
PPP1CA
CAMK2G
PPP1CC
CAMK2D
CAMK2B
GRB2
D
si-Control
si-PEAK1
si-PEAK2
PEAK1
PEAK2
β-actin
E
si-PEAK1
si-Control
Antibodies
CAMK2D /PEAK1
CAMK2G /PEAK1
Dots per cell
F
si-PEAK2
si-Control
CAMK2D /PEAK2
CAMK2G /PEAK2

Figure 1. Identification of specific CAMK2 isoforms as PEAK1/2 interactors via BiCAP-MS/MS. A-C. Results of BiCAP-MS/MS screen. Volcano plots indicate enriched interactors for the PEAK1 homotypic complex (A), PEAK2 homotypic complex (B) and PEAK1/PEAK2 heterotypic complex (C). The known PEAK1 interactor Grb2 and targets of particular interest, including specific CAMK2 family members, are highlighted in blue. Dotted lines indicate fold change and p value cut-offs. **D. Western blotting validation of PEAK1 and PEAK2 knockdown.** PEAK1 and PEAK2 were knocked down using siRNA pools, with successful knockdown confirmed by Western blotting. **E-F. Validation of PEAK1/2 association with CAMK2D and CAMK2G by proximity ligation assays.** Left panels, representative proximity ligation assay (PLA) images from MDA-MB-231 cells for interaction of PEAK1 (E) or PEAK2 (F) with CAMK2D and CAMK2G. Cells were transfected with either si-PEAK1 (E), si-PEAK2 (F) or si-Control. Right panels, quantification of protein interactions in each cell. The data are expressed as dot number divided by cell number. In each condition, more than 50 cells have been counted. Error bars represent the standard error of the mean from n=3 independent experiments. * = $p < 0.05$, ** = $p < 0.01$ by student's t-test.

Figure 2.

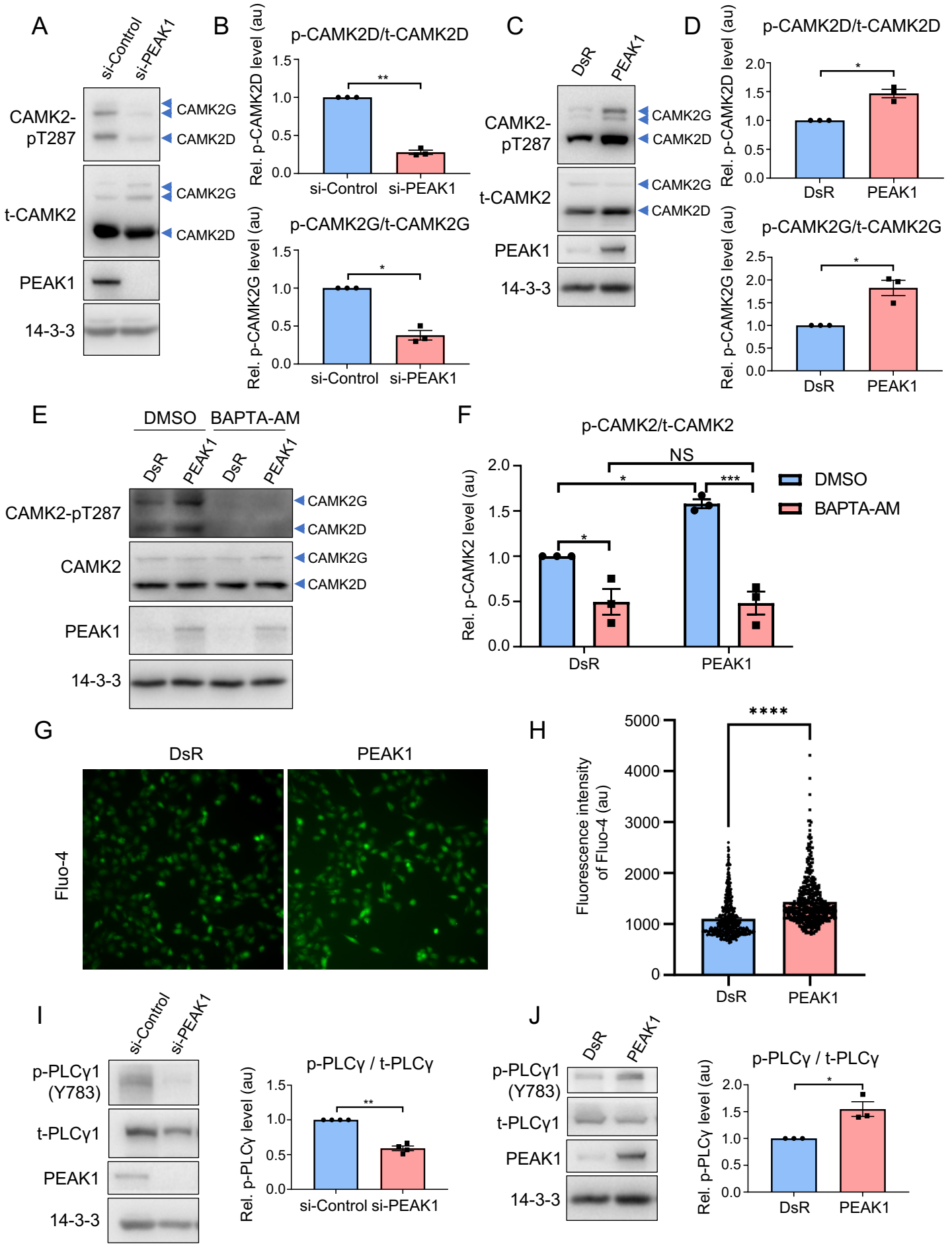
A
si-Control
si-PEAK1
CAMK2-pT287
CAMK2G
CAMK2D
t-CAMK2
CAMK2G
CAMK2D
PEAK1
14-3-3
B
p-CAMK2D/t-CAMK2D
Rel. p-CAMK2D level (au)
1.5
1.0
0.5
0.0
**
si-Control
si-PEAK1
p-CAMK2G/t-CAMK2G
Rel. p-CAMK2G level (au)
1.5
1.0
0.5
0.0
*
si-Control
si-PEAK1
C
DsR
PEAK1
CAMK2-pT287
CAMK2G
CAMK2D
t-CAMK2
CAMK2G
CAMK2D
PEAK1
14-3-3
D
p-CAMK2D/t-CAMK2D
Rel. p-CAMK2D level (au)
2.0
1.5
1.0
0.5
0.0
*
DsR
PEAK1
p-CAMK2G/t-CAMK2G
Rel. p-CAMK2G level (au)
2.5
2.0
1.5
1.0
0.5
0.0
*
DsR
PEAK1
E
DMSO
BAPTA-AM
DsR
PEAK1
DsR
PEAK1
CAMK2-pT287
CAMK2G
CAMK2D
CAMK2
CAMK2G
CAMK2D
PEAK1
14-3-3
F
p-CAMK2/t-CAMK2
Rel. p-CAMK2 level (au)
2.0
1.5
1.0
0.5
0.0
NS
*
***
*
DMSO
BAPTA-AM
DsR
PEAK1
G
DsR
PEAK1
Fluo-4
H
Fluorescence intensity of Fluo-4 (au)
5000
4000
3000
2000
1000
0
****
DsR
PEAK1
I
si-Control
si-PEAK1
p-PLCγ1 (Y783)
t-PLCγ1
PEAK1
14-3-3
p-PLCγ / t-PLCγ
Rel. p-PLCγ level (au)
1.5
1.0
0.5
0.0
**
si-Control
si-PEAK1
J
DsR
PEAK1
p-PLCγ1 (Y783)
t-PLCγ1
PEAK1
14-3-3
p-PLCγ / t-PLCγ
Rel. p-PLCγ level (au)
2.0
1.5
1.0
0.5
0.0
*
DsR
PEAK1

Figure 2. PEAK1-mediated regulation of CAMK2 activity in triple negative breast cancer cells. A-D. Manipulation of PEAK1 expression modulates CAMK2 activity. PEAK1 was knocked down using a siRNA (A-B) or overexpressed via transient transfection (C-D) in MDA-MB-231 cells and autonomous activation of CAMK2 determined by Western blotting as indicated. Blotting for 14-3-3 served as a loading control. Histograms indicate CAMK2 T287 phosphorylation normalized for total CAMK2 expression, with 'au' indicating arbitrary units. **E-F. PEAK1-promoted CAMK2 activation is calcium-dependent.** MDA-MB-231 cells were transfected with a PEAK1 construct in the presence or absence of 10 μM BAPTA-AM. Cell lysates were Western blotted as indicated (E) and CAMK2 activation quantified as above for CAMK2D/G combined (F), with data expressed relative to the DsR (vector)/DMSO control which was arbitrarily set at 1. **G-H. Overexpression of PEAK1 increases intracellular Ca^{2+}.** MDA-MB-231_EcoR cells stably overexpressing PEAK1 were loaded with calcium-sensitive dye Fluo-4 AM and then imaged with a fluorescence microscope. Representative images from 3 independent experiments are shown (G) as well as quantification of Fluo-4 images (H), presented as mean Fluo-4 fluorescence ± SEM. These are representative data from one biological replicate from a total of three. **I-J. PEAK1 regulates tyrosine phosphorylation of PLCγ1.** MDA-MB-231 cells were transfected with PEAK1 siRNA (I) or a PEAK1 expression vector (J) and then cell lysates were Western blotted as indicated. The histograms indicate Y783-phosphorylated PLCγ1 normalized for total PLCγ1 expression. For all panels, error bars represent the standard error of the mean from n=3 independent experiments. NS indicates $p > 0.05$, * = $p < 0.05$, ** = $p<0.01$, *** = $p<0.001$, ****, $p < 0.0001$, by ratio paired t-test (B, D, I, J), two-way ANOVA with Tukey's multiple comparisons test (F), or unpaired t-test (H).

Figure 3.

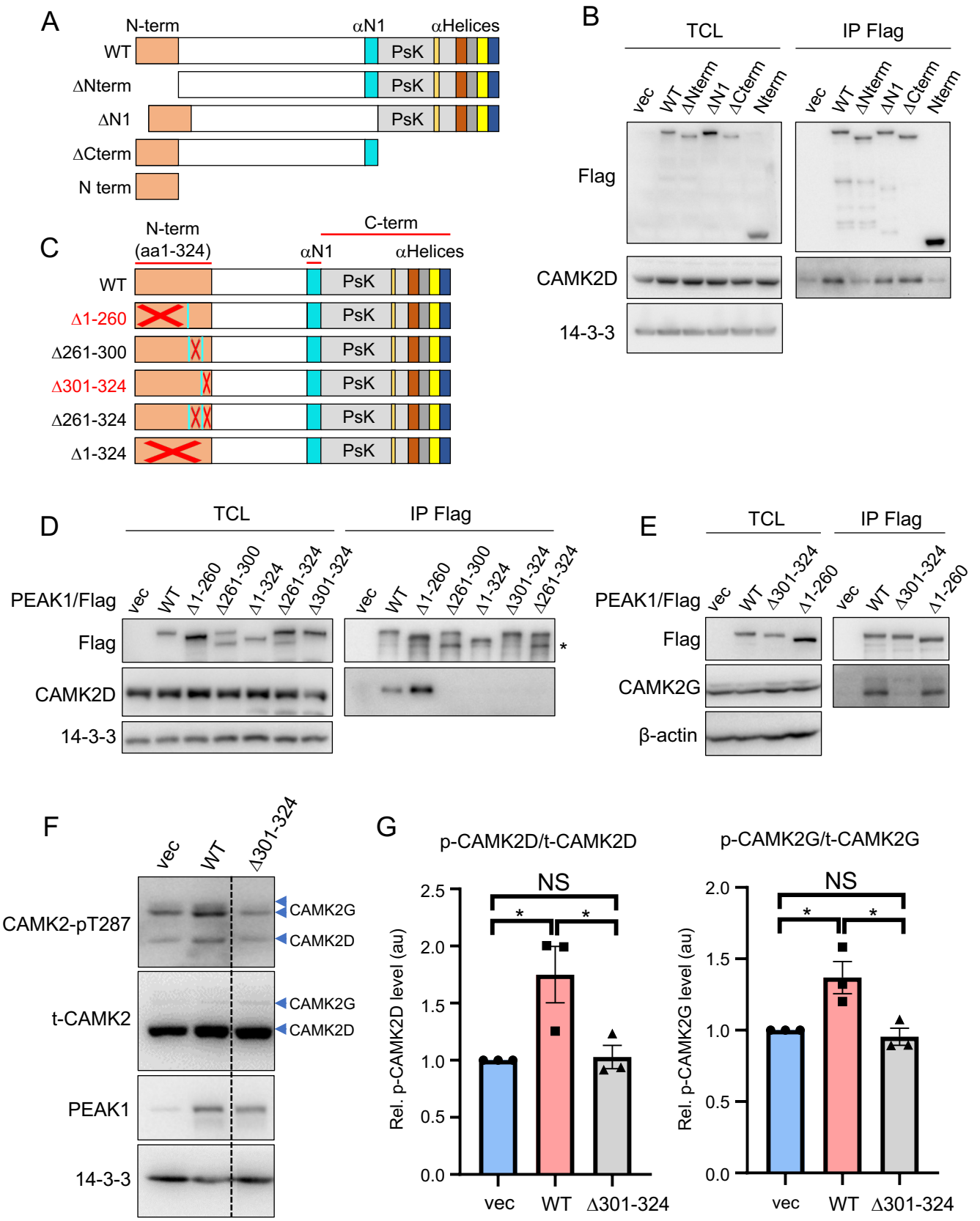
A
N-term
αN1
αHelices
WT
ΔNterm
ΔN1
ΔCterm
N term
PsK
B
TCL
IP Flag
vec
WT
ΔNterm
ΔN1
ΔCterm
Nterm
Flag
CAMK2D
14-3-3
C
N-term
(aa1-324)
C-term
αN1
αHelices
WT
Δ1-260
Δ261-300
Δ301-324
Δ261-324
Δ1-324
PsK
D
TCL
IP Flag
PEAK1/Flag
vec
WT
Δ1-260
Δ261-300
Δ1-324
Δ261-324
Δ301-324
Flag
CAMK2D
14-3-3
*
E
TCL
IP Flag
PEAK1/Flag
vec
WT
Δ301-324
Δ1-260
Flag
CAMK2G
β-actin
F
vec
WT
Δ301-324
CAMK2-pT287
t-CAMK2
PEAK1
14-3-3
CAMK2G
CAMK2D
G
p-CAMK2D/t-CAMK2D
Rel. p-CAMK2D level (au)
NS
*
*
2.5
2.0
1.5
1.0
0.5
0.0
vec
WT
Δ301-324
p-CAMK2G/t-CAMK2G
Rel. p-CAMK2G level (au)
NS
*
*
2.0
1.5
1.0
0.5
0.0
vec
WT
Δ301-324

Figure 3. Mapping the CAMK2 binding region on PEAK1. A. Schematic structure of PEAK1 and various truncation mutants. WT, wildtype. **B. Association of CAMK2D with specific PEAK1 deletion mutants.** The indicated Flag-tagged PEAK1 deletion mutants were expressed in HEK293T cells. Total cell lysates (TCL) and Flag IPs were subjected to Western blotting as indicated. **C. Schematic representation of various PEAK1 N-terminal deletion mutants.** Deleted regions of PEAK1 are indicated by red crosses. **D-E. Fine structure mapping of N-terminal regions required for the association of PEAK1 with CAMK2D (D) or CAMK2G (E).** Analysis was undertaken as in (B). The asterisk in 3D highlights degradation products present for the Δ261-300 and Δ261-324 mutants. **F-G. PEAK1 binding to CAMK2 is required for CAMK2 activation.** MDA-MB-231 cells were transfected with WT PEAK1 or the Δ301-324 PEAK1 construct. Cell lysates were Western blotted as indicated (F), with the dotted line in F indicating where the image was cropped to remove an irrelevant lane. Raw data for the full image accompanies the manuscript. Relative CAMK2 activation, as determined by T287 phosphorylation, was then quantified (G). Data are expressed relative to vector control which was arbitrarily set at 1. All data in B, D and E are representative of at least 2 independent experiments. In G, error bars represent the standard error of the mean from n=3 independent experiments. NS indicates $p > 0.05$, * = $p < 0.05$ by one-way ANOVA with Tukey's multiple comparisons test.

Figure 4.

A

									-9					-5					-3					0	
GluN2B	-	-	-	-	-	-	-	-	R	-	N	K	-	L	-	-	R	-	R	Q	-	H	S	Y	D
Tiam1	R	T	L	D	S	H	A	S	R	M	T	Q	-	L	-	-	K	-	K	Q	-	A	A	L	-
densin-180	-	-	-	-	-	S	H	G	R	-	R	P	-	L	-	-	I	-	R	Q	D	R	I	V	G
GluA1	-	-	-	-	S	K	R	M	K	G	F	C	-	L	-	-	I	-	P	Q	-	Q	S	I	N
CAMKIIN	-	-	-	-	-	-	-	K	R	-	P	P	K	L	G	Q	I	G	R	S	-	K	R	V	V
PEAK1	K	K	W	N	T	I	P	L	R	-	N	K	S	L	-	Q	-	-	R	I	-	C	A	V	D
									R297					L301					R303						

B

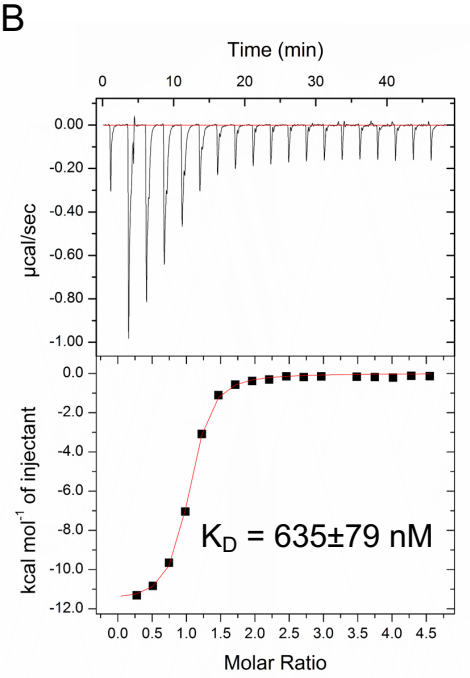

C

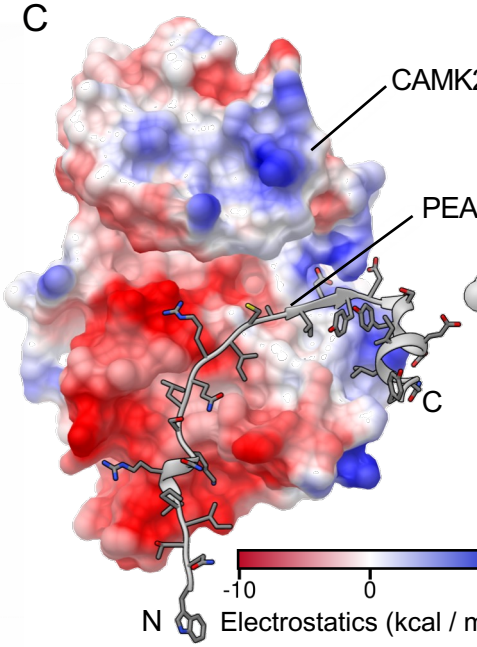

D

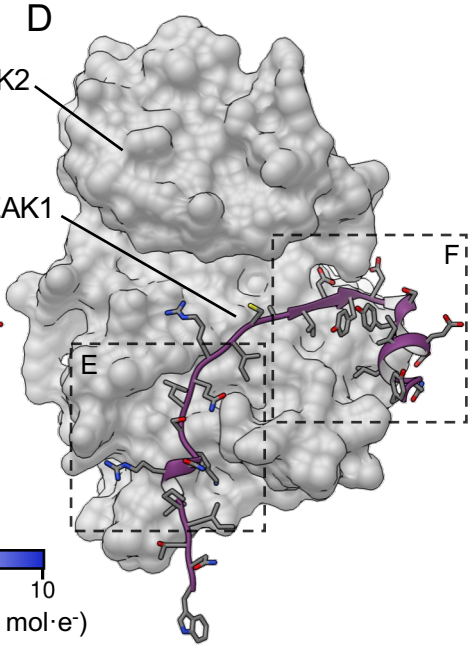

E

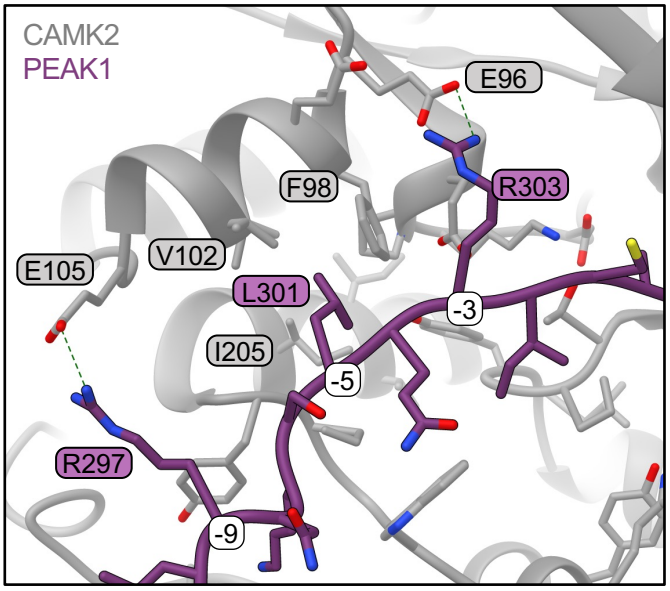

F

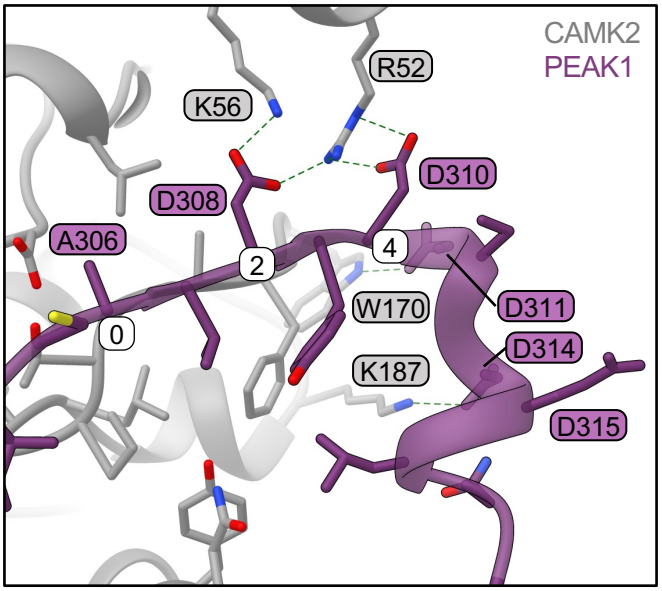

Figure 4. Characterization of a conserved CAMK2 interaction motif (CIM) on PEAK1. A. Sequence alignment of the PEAK1 CIM with other CAMK2 binding partners. The critical residues for CAMK2 interaction (R297, L301 and R303 in PEAK1) are highlighted in yellow. The canonical motif numbering (A306 being 0) is shown above the alignment. **B. Representative ITC measurement of CAMK2 kinase domain binding to PEAK1 CIM peptide.** The mean Kd value from n=3 independent experiments is indicated. **C. Comparative modelling of the PEAK1/CAMK2 interaction by AlphaFold.** Surface representation of CAMK2 with PEAK1 amino acids 291-320 shown as ribbon (grey). The orientation is as in Supp Figure 6. CAMK2 is coloured by electrostatic charge. The PEAK1 binding site on CAMK2 is noticeably negative, with key arginine residues of PEAK1 mediating interactions with CAMK2. The N- and C-termini are labelled as N and C, respectively. **D. Surface representation of modelled PEAK1/CAMK2 interaction.** CAMK2 is grey and PEAK1 amino acids 291-320 are purple. **E-F. Focused view of key predicted molecular interactions.** Boxed regions from (D) illustrating predicted formation of salt bridges and electrostatic interactions (dotted lines) by specific PEAK1 residues across the surface of CAMK2. The canonical numbering of the PEAK1 motif is shown in white boxes.

Figure 5

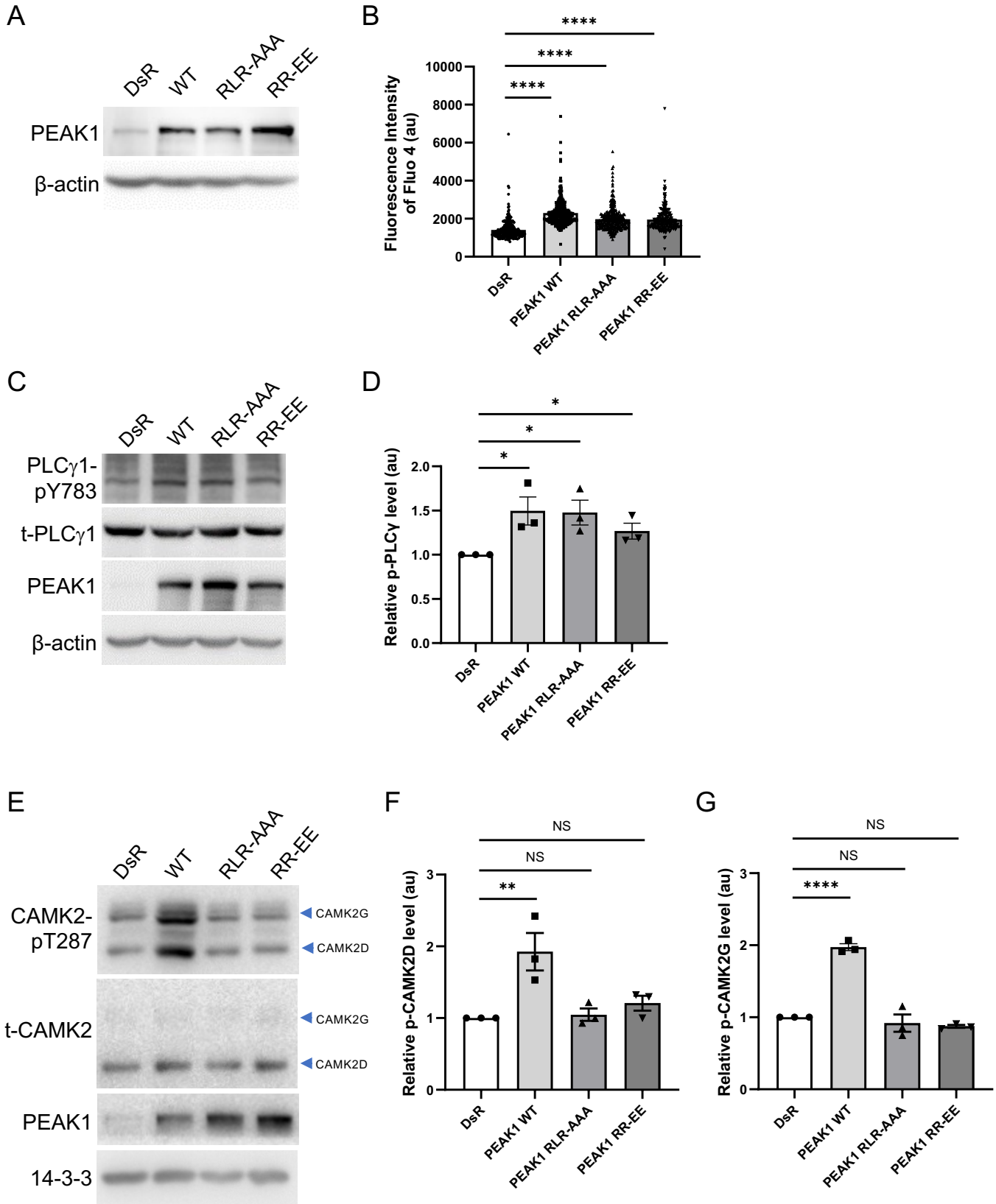
A
DsR
WT
RLR-AAA
RR-EE
PEAK1
β-actin
B
****
****
****
Fluorescence Intensity of Fluo 4 (au)
10000
8000
6000
4000
2000
0
DsR
PEAK1 WT
PEAK1 RLR-AAA
PEAK1 RR-EE
C
DsR
WT
RLR-AAA
RR-EE
PLCγ1-pY783
t-PLCγ1
PEAK1
β-actin
D
*
*
*
Relative p-PLCγ level (au)
2.0
1.5
1.0
0.5
0.0
DsR
PEAK1 WT
PEAK1 RLR-AAA
PEAK1 RR-EE
E
DsR
WT
RLR-AAA
RR-EE
CAMK2-pT287
CAMK2G
CAMK2D
t-CAMK2
CAMK2G
CAMK2D
PEAK1
14-3-3
F
NS
NS
**
Relative p-CAMK2D level (au)
3
2
1
0
DsR
PEAK1 WT
PEAK1 RLR-AAA
PEAK1 RR-EE
G
NS
NS
****
Relative p-CAMK2G level (au)
3
2
1
0
DsR
PEAK1 WT
PEAK1 RLR-AAA
PEAK1 RR-EE

Figure 5. The role of the PEAK1 CIM in CAMK2 activation. A-B. Effect of CIM mutation on intracellular Ca^{2+} levels. Constructs expressing WT PEAK1 or the indicated mutants were stably expressed in MDA-MB-231_EcoR cells via retroviral transduction. PEAK1 expression levels were determined by Western blot (A) and Ca^{2+} levels (B) assayed as in Figure 2G-H. Data in B represent mean Fluo-4 fluorescence ± SEM from one representative biological replicate from a total of two independent experiments. Statistical analysis utilized one way ANOVA with Dunnett's multiple comparisons test with **** indicating $p < 0.0001$. **C-D. Effect of CIM mutation on tyrosine phosphorylation of PLCγ1**. The indicated plasmids were transiently transfected into HEK293 cells and cell lysates Western blotted as indicated (C). PLCγ1 tyrosine phosphorylation was normalized for total expression (D). Data in D are expressed relative to the vector control which was arbitrarily set at 1 and represent the mean ± SEM of 3 independent biological replicates, * indicates $p<0.05$ by unpaired t-test. **E-G. Effect of CIM mutation on CAMK2 activation.** Plasmids encoding WT PEAK1 and the indicated mutants were transfected into MDA-MB-231 cells. Total cell lysates were Western blotted as indicated (E) and then relative CAMK2 activation was quantified (F-G). Data are expressed relative to the vector (DsR) control which was arbitrarily set at 1. NS indicates $p > 0.05$, ** = $p < 0.01$ and **** = $p < 0.0001$ by one-way ANOVA with Dunnett's multiple comparisons test.

Figure 6.

A

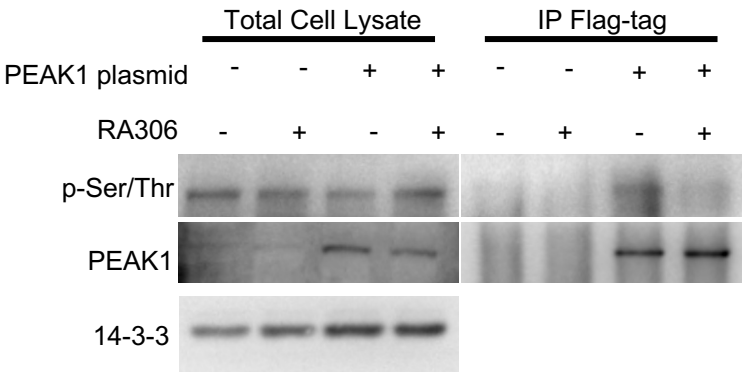

B

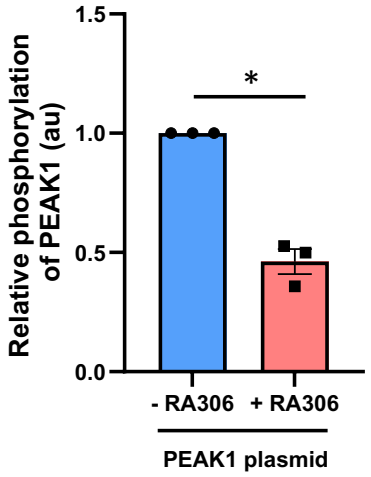

C

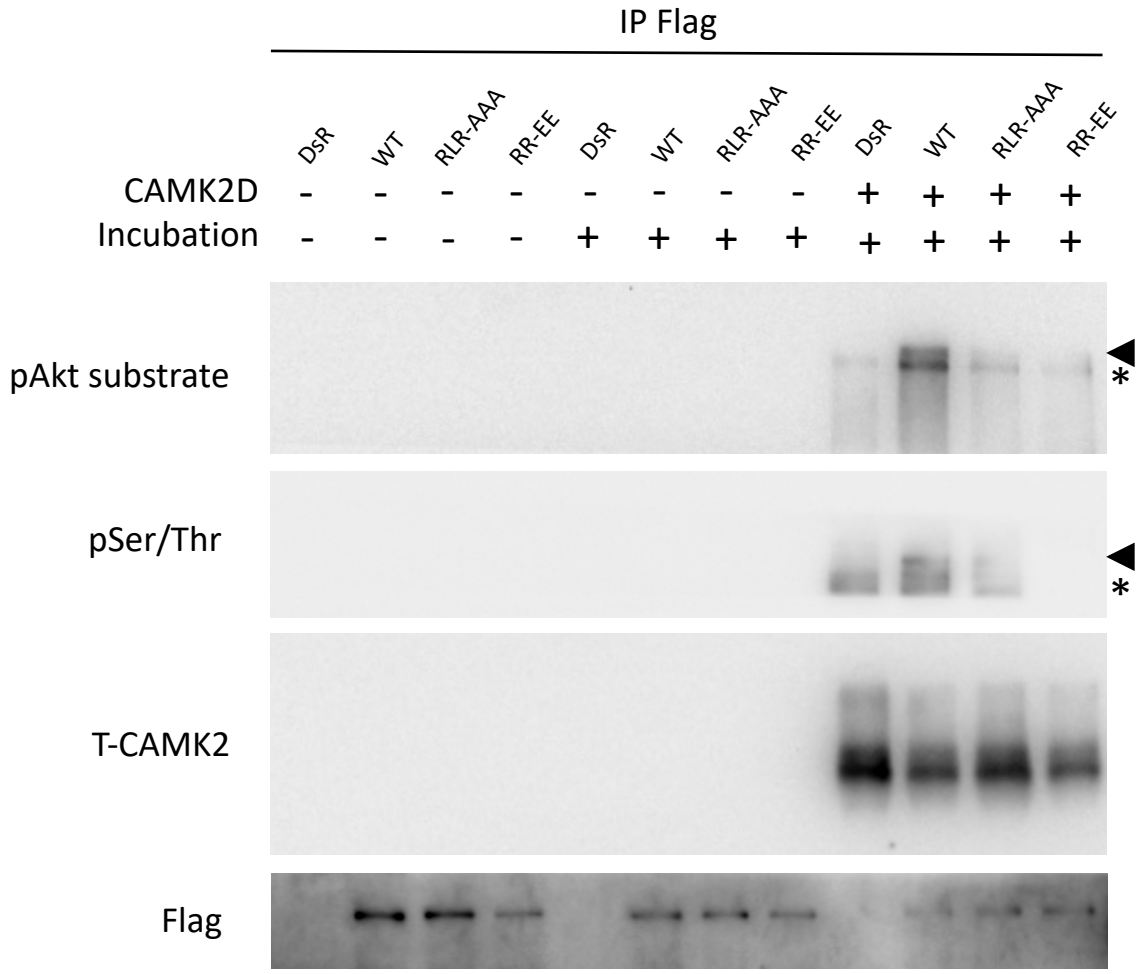

D

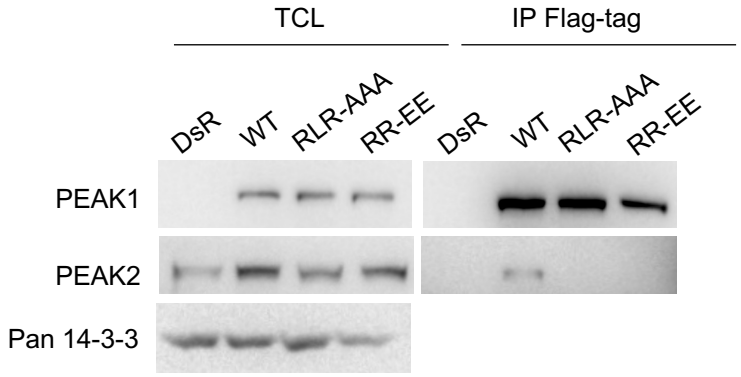

Figure 6. CAMK2 phosphorylates PEAK1 to regulate the PEAK1 interactome. A-B. RA306 inhibits PEAK1 serine/threonine phosphorylation. MDA-MB-231_EcoR cells stably expressing Flag-tagged PEAK1 were treated with RA306 (1 μM) for 24 h and cell lysates were directly Western blotted or subject to immunoprecipitation with Flag antibody prior to blotting as indicated (A). Relative serine/threonine phosphorylation of PEAK1, normalized for total PEAK1, is shown in the histogram (B). **C. CAMK2 phosphorylates PEAK1 *in vitro*.** Flag-tagged versions of WT and mutant PEAK1 proteins were expressed in HEK293T cells. PEAK1 proteins were immunoprecipitated using anti-Flag antibody and following washing, immediately treated with SDS-PAGE sample buffer (SB) (no incubation) or incubated in kinase reaction buffer supplemented as indicated at 37ºC for 30 min. Reactions were terminated with SB. Samples were then Western blotted as indicated. The asterisk indicates a background band present in all CAMK2D-incubated samples including the vector control while the arrowhead highlights phosphorylated PEAK1. **D. Impact of CIM mutations on heterotypic association with PEAK2.** Flag-tagged WT PEAK1 or PEAK1 mutants were expressed in MDA-MB-231 cells and association with endogenous PEAK2 assayed by IP/Western. For panel B, * = $p<0.05$ by ratio paired t-test.

Figure 7

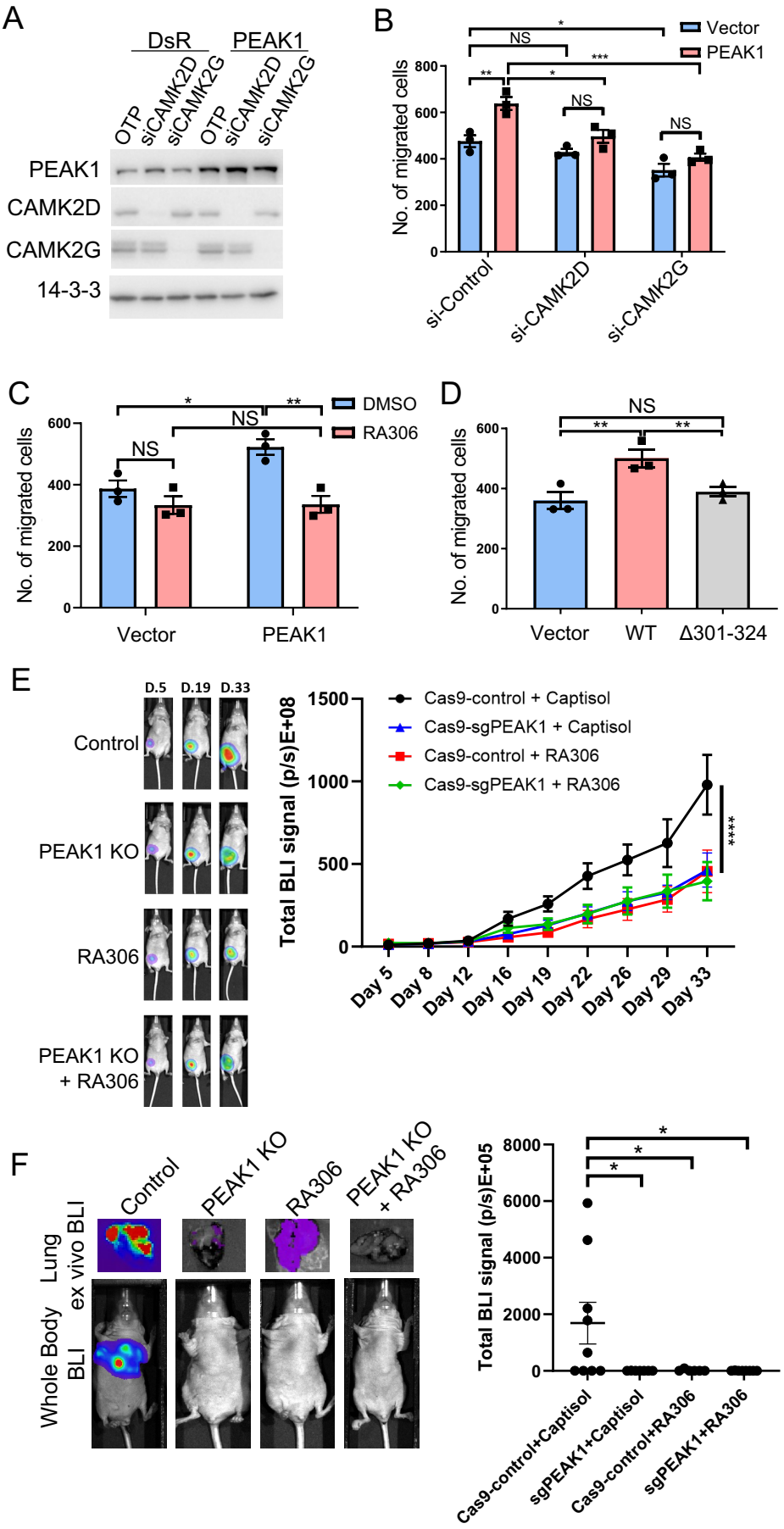
A
DsR
PEAK1
OTP
siCAMK2D
siCAMK2G
OTP
siCAMK2D
siCAMK2G
PEAK1
CAMK2D
CAMK2G
14-3-3
B
Vector
PEAK1
No. of migrated cells
si-Control
si-CAMK2D
si-CAMK2G
NS
C
DMSO
RA306
No. of migrated cells
Vector
PEAK1
D
No. of migrated cells
Vector
WT
Δ301-324
E
D.5
D.19
D.33
Control
PEAK1 KO
RA306
PEAK1 KO
+ RA306
Total BLI signal (p/s)E+08
Cas9-control + Captisol
Cas9-sgPEAK1 + Captisol
Cas9-control + RA306
Cas9-sgPEAK1 + RA306
Day 5
Day 8
Day 12
Day 16
Day 19
Day 22
Day 26
Day 29
Day 33
F
Control
PEAK1 KO
RA306
PEAK1 KO
+ RA306
Lung
ex vivo BLI
Whole Body
BLI
Total BLI signal (p/s)E+05
Cas9-control+Captisol
sgPEAK1+Captisol
Cas9-control+RA306
sgPEAK1+RA306

Figure 7. Role of CAMK2 in PEAK1-regulated biological endpoints in TNBC models. A. PEAK1 overexpression in combination with CAMK2D and CAMK2G knockdown in MDA-MB-231 cells. Cells were transfected with a PEAK1 plasmid in the presence or absence of siRNA-mediated CAMK2D or CAMK2G knockdown. Cell lysates were Western blotted as indicated. **B. Role of CAMK2D/G in PEAK1-promoted MDA-MB-231 cell migration.** Cells validated in (A) were subjected to a transwell migration assay. **C-D**, **Role of CAMK2 activation.** MDA-MB-231 cells were transfected with a PEAK1 plasmid and subject to transwell migration assays in the presence or absence of RA306 (C)**.** Plasmids expressing WT PEAK1 and the Δ301-324 mutant that cannot activate CAMK2 were transiently transfected into MDA-MB-231 cells, and cells were subjected to a transwell migration assay (D). **E. Role of PEAK1/CAMK2 signalling in TNBC xenograft growth.** Control MDA-MB-231_HM cells (Cas9-control) or PEAK1 KO cells (Cas9-sgPEAK1) in combination with RA306 or vehicle control (captisol) were injected into the mammary fat pad. Left panel, representative whole body bioluminescent imaging (BLI) images from each group at different time points as indicated. Right panel, quantification of xenograft growth. Each treatment group exhibited ≥ 9 mice. **F. Role of PEAK1/CAMK2 signalling in TNBC metastasis.** Control MDA-MB-231_HM cells (Cas9-control) or PEAK1 KO cells (Cas9-sgPEAK1) in combination with RA306 or vehicle control (captisol) were injected into the mammary fat pad. At Day 19 post-injection when the primary tumour from each group reached ~ 100 mm^3, they were resected, and tumour growth at secondary sites was measured. Left panel, representative whole body and *ex vivo* lung BLI images from each group at Day 72 post injection. Right panel, luciferase intensities of tumour metastasis to lung were generated from each group. Error bars represents the standard error of the mean from n=3 independent experiments (B-D) or from the individuals of each group (E & F). NS indicates $p > 0.05$, * = $p < 0.05$, ** = $p < 0.01$, *** = $p < 0.001$, **** = $p < 0.0001$ by two-way ANOVA with Tukey's multiple comparisons test (B, C, E), one-way ANOVA with Tukey's multiple comparisons test (D), or one-way ANOVA with Dunnett's multiple comparisons test (F).

Figure 8.

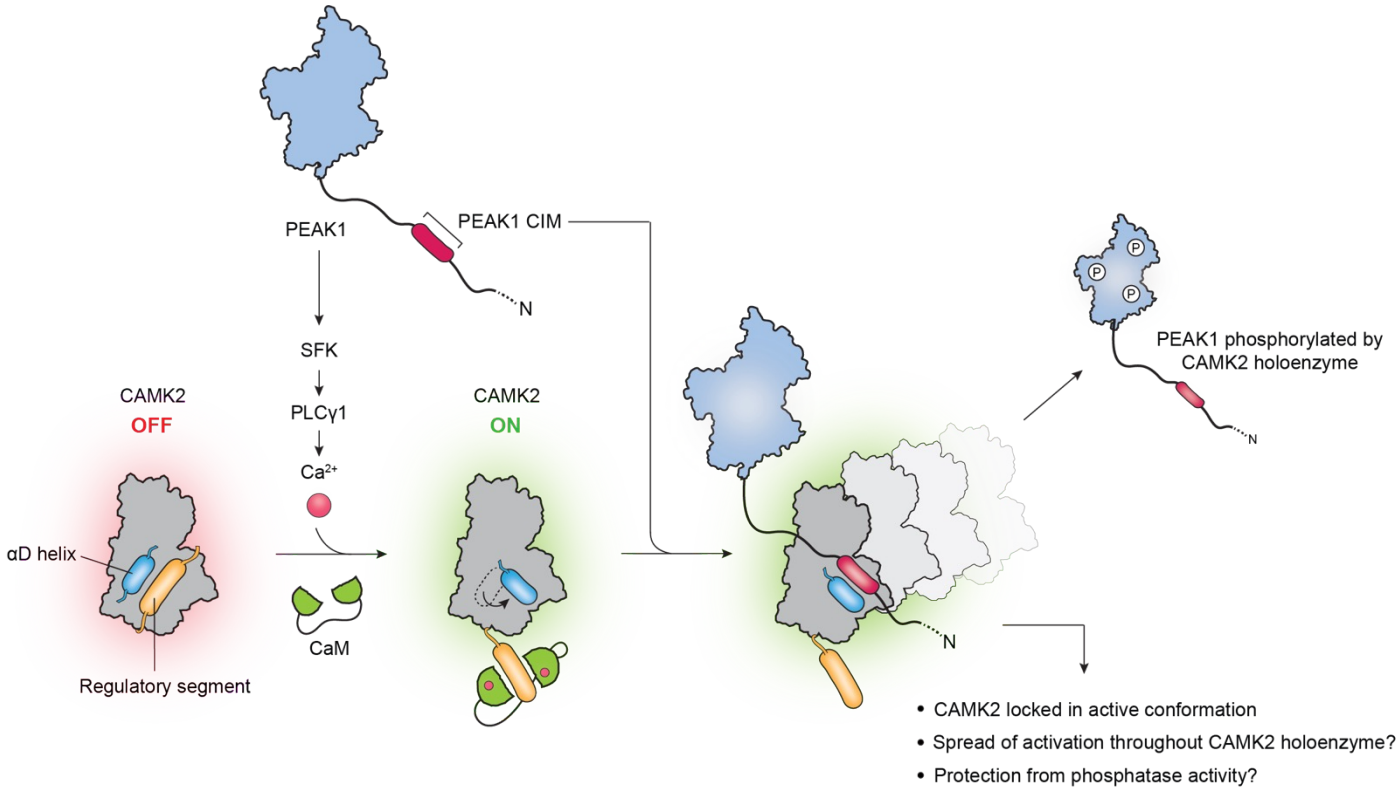

Figure 8. Schematic representation of feed-forward regulation of CAMK2 by PEAK1. PEAK1 enhances intracellular Ca^{2+} by promoting SFK-mediated tyrosine phosphorylation of PLCγ1. This leads to classical activation of CAMK2 by Ca^{2+}/CaM and the αD helix rotates out. The PEAK1 CIM then binds to the CAMK2 substrate binding site and competes with the regulatory segment, effectively 'locking' CAMK2 in an active conformation. Sustained phosphorylation of PEAK1 and CAMK2 itself (on T287) then occurs as the PEAK1 CIM undergoes cycles of dissociation and re-association. However, other mechanisms may contribute to the observed effects on CAMK2 activation, as indicated on the figure. CIM-mediated recruitment of PEAK1 to the CAMK2 holoenzyme promotes serine/threonine phosphorylation of PEAK1 which in turn positively regulates heterotypic association with PEAK2.